ISSN0736-5306

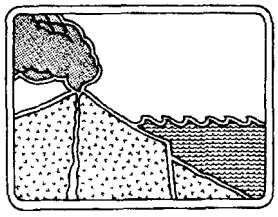

SCIENCE OF TSUNAMI HAZARDS

The International Journal of The Tsunami Society

Volume 18 Number 2 2000

OBJECTIVE: **The Tsunami Society** publishes this journal to increase and disseminate knowledge about tsunamis and their hazards.

DISCLAIMER: Although these articles have been technically reviewed by peers, **The Tsunami Society** is not responsible for the veracity of any statement , opinion or consequences.

Submit manuscripts of articles, notes or letters to the Editor. If an article is accepted for publication the author(s) must submit a camera ready manuscript in the journal format. A voluntary $30.00 page charge for Tsunami Society members, $50.00 for non-members will include 50 reprints.

SUBSCRIPTION INFORMATION: Price per copy $50.00 USA

 Previous issues of the journal are available in PDF format at **http://epubs.lanl.gov/tsunami/** and on a CD-ROM from the Society.

ISSN 0736-5306 **http://www.ccalmr.ogi.edu/STH**

Published by The Tsunami Society in Honolulu, Hawaii, USA

TWENTIETH CENTURY Ms AND Mw VALUES AS TSUNAMIGENIC INDICATORS FOR HAWAII

Daniel A. Walker

Tsunami Memorial Institute

59-530 Pupukea Road

Haleiwa, Hawaii 96712

ABSTRACT

More than two hundred earthquakes from 1900 through 1999 with epicenters along margins of the Pacific are analyzed in terms of their surface wave magnitudes, moment magnitudes, and possible tsunamigenic effects in Hawaii. Data for regions which have not produced significant tsunamis in Hawaii are found to have generally smaller moment magnitudes than have occurred in regions which have produced significant tsunamis in Hawaii. These findings suggest that an accurate assessment of the destructive potential of additional portions of the circum-Pacific arc could only be determined if earthquakes with large moment magnitudes were to occur in those areas. Also, the past one hundred years of surface wave magnitude, moment magnitude, and runup data provides for the determination of conservative estimates of tsunamigenic thresholds in Hawaii for earthquakes occurring in most regions of the Pacifc.

Introduction

In an earlier report (Walker, 1997) surface wave magnitudes (MS) and seismic moments (MO) were regionally analyzed for evidence of tsunamigenic thresholds in the Pacific. In the absence of sufficient data, only rough estimates could be made for some of the regions investigated. In this report data through 1999 have been added, moments have been converted to moment magnitudes (Mw), and regions have been combined to provide a larger data base on which to estimate thresholds.

MS and Mw for Pacific-Wide Tsunamis

Table 1 is a listing of all earthquakes producing reported runups of 0.1 meters or more in Hawaii. Available surface wave magnitudes and moment magnitudes, as well as maximum reported runups in the main Hawaiian Islands are also listed. Most destructive tsunamis in Hawaii have their source locations in the North Pacific or in South America, with little or no destructive effects from tsunamis originating in other regions. An important question is whether these regions are truly incapable of producing destructive tsunamis in Hawaii or whether earthquakes from these regions will eventually have the assemblage of parameters (i.e., magnitudes, source dimensions, source orientations, and travel paths) necessary for destructive runups in Hawaii. Surface wave magnitudes, moment magnitudes, and runups for the events listed in Table 1 are plotted in Figures 1 and 2. Data in columns to the left are for earthquakes in "tsunamigenic regions" and data in columns to the right are for earthquakes in "non-tsunamigenic regions". The only obvious difference in the data for these two regions is that in the "non-tsunamigenic regions" earthquakes generally have smaller moment magnitudes. This observation suggests that destructive runups could be recorded in Hawaii if these regions were to have earthquakes with moment magnitudes comparable to those observed in the North Pacific or South America. Looking vertically up the columns of values in Figures 1 and 2, it is obvious that for any given surface wave magnitude, events with greater moment magnitudes have larger tsunamis.

The data also provides useful guidelines for assessing tsunamigenic potential, With these guidelines, the probability of missed tsunamis and the frequency of false tsunami warnings could be reduced. This is an important consideration until such time as the reliability of warnings based on deep ocean gauges, other instrumentation, and numerical modeling can be established.

Figure 1 also confirms the well-known fact that large earthquakes, in terms of Ms and/or Mw, are generally more likely to produce large tsunamis than smaller earthquakes. However, there is no direct or perfect correlation between runup values and surface wave magnitudes or moment magnitudes. Earthquakes with large surface wave magnitudes can have small runups (e.g., Aleutians, 1938, 8.1Ms, 0.3m; Table 1), while earthquakes with smaller MS's can have larger runups (e.g., Aleutians, 1946, 7.1Ms, 16.4 m). Also, earthquakes with large moment magnitudes can have small runups (e.g., Mexico, 1985, 8.0 Mw, 0.1m), while earthquakes with smaller Mw's can have larger runups (e.g., Mexico, 1932, 7.9Mw, 0.4m). Such discrepancies could be substantially resolved

through considerations of other parameters (i.e., source dimensions, source orientations, and travel paths). Roughly half of the data points above the lines in Figures 1 and 2 are for earthquakes which generated significant, potentially destructive tsunamis in Hawaii. All of the data points below the line are for earthquakes which did not generate Pacific-wide tsunamis or which generated only moderate or small Pacific-wide tsunamis.

Other Data Points and Considerations

The 1946 event (7.1 Ms, 8.0 Mw, 16.4m) remains as the most enigmatic tsunami of the twentieth century (Fryer et al., 2000). Its relatively moderate surface wave magnitude and much larger moment magnitude are unique and suggest that moderate earthquakes with similar "deficits" (Fryer, 1996) could be extremely dangerous regardless of whether such "tsunami earthquakes" (Kanamori, 1972; Fukao, 1979; Talandier and Okal, 1989) are generated by massive submarine landslides, slow ruptures, or liquifaction of submarine sediments (Walker, 1992).

The data point at 7.1Ms, 7.7 Mw has an epicenter in Peru that appears to be east of the crest of the Andes. This event, which occurred on 1 November 1947, was probably too far inland to generate a measurable tsunami. The data point at 7.7 Ms, 8.0 Mw has an epicenter in New Guinea which may also be too far inland to produce a tsunami. This earthquake occurred on 20 September 1935. It should also be noted that extensive surveys of runups for significant tsunamis in Hawaii only began with the 1946 tsunami, Therefore, some larger runups may have been missed in large tsunamis occurring prior to 1946.

The only data point deleted from the listings used in this study is an event in Lander and Lockridge (1989) which occurred in 1901 . This earthquake is reported to have occurred in Tonga, yet its coordinates (22 S, 170 E) indicate an epicenter much further west in Vanuatu. [Tonga is near 20 S, 170 W.] Pacheco and Sykes (1992) give the location as Vanuatu , as does the National Earthquake Information Services internet listing of "Significant Worldwide Earthquakes". Runup or tide gauge readings were 1.2m at Hoopuloa and Kailua on the Big Island and 0. lm in Honolulu. In the descriptive narrative of Lander and Lockridge (p. 32) the following statement can be found. "The travel times to both Kailua and Honolulu fit a source region near the Tonga Islands. However, inquiries to Apia and Fiji did not uncover any reports of local observations." For other subsequent earthquakes in Vanuatu of roughly comparable magnitudes (1920, 1934, 1966, and 1980) only one was reported with runups in Hawaii, that being a 0.1 m reading in Kailua on the Big Island. Examination of local newspaper accounts (the *Hawaiian Star* and *Evening Bulletin,* both of 13 August 1901) indicate that the wave moved progressively southward down the western coastline of the Big Island starting at Kailua. Word of the approaching wave was sent by telephone to the southeastern coast. However, by the time the wave was to have reached those areas, it did not have sufficient energy to be observed. Any tsunami originating in Vanuatu with significant runups on the western coast of the Big Island should also be observed along the southeastern coast. In view of these considerations, it may be reasonable to suggest that the runups were associated with a submarine landslide off the Kona Coast. Such an event occurred in 1919 with a reported maximum runup of 4.3 m in the same area (at Hoopuloa). As with the 1901 event, no local earthquake was felt or reported at the time of the 1919 tsunami.

In this century a number of large earthquakes have occurred in marginal seas and oceans of the South Pacific (i.e., the Philippines, Banda Sea, Molucca Passage, Java, Cotabato, and the Macquarie Ridge). None had either surface wave magnitudes in excess of 8.2 or moment magnitudes in excess of 8.4. Although some of these generated destructive local tsunamis, none were reported in Hawaii. Reported tsunamis in Hawaii may be possible for some of these regions if the moment magnitudes for their earthquakes exceed 8.4. Also, the potential for the recording of tsunamis in Hawaii for smaller earthquakes from other locations in these regions can not be discounted in the absence of detailed modeling studies.

Conclusions

Diverse margins of the Pacific which have not yet produced destructive tsunamis in Hawaii may cause such destruction if the moment magnitudes of their earthquakes are comparable to some of the larger twentieth century earthquakes that originated in the North Pacific or South America.

Tf Figures 1 and 2 were data for circum-Pacific earthquakes in the twenty-first century and warnings were to be called for all of these earthquakes, only eleven might be viewed by the public as valid and seventy-two would be considered as false alarms. Such a system would adequately warn of destructive tsunamis, but eventually few would pay any attention to those valid warnings because of the large number of false alarms.

Until such time as runups can be reliably predicted from numerical modeling of data recorded by deep ocean gauges and other instruments, warning systems must accept the possibility, however remote, that a somewhat dangerous tsunami could strike some areas of the Hawaiian Islands with no warning having been issued.

Failure to acknowledge this fact would be a failure to acknowledge reality, and attempts to avoid every possibility of a "missed" tsunami would ensure the destruction of any such warning system because of excessive false warnings. The data presented here provides guidelines by which false warnings can be reduced without substantially increasing the risks of missed tsunamis.

Acknowledgments. I would like to thank all those whose field investigations and research have provided the data on which our current knowledge is based.

REFERENCES

Fryer, G J. (1997). Magnitude deficits and the tsunamigenic potential of an earthquake, *Seism. Res. Letters 68, 292.*

Fryer, G. J., P. Watts, L. F. Pratson, and J. V. Gardner (2000). 1 April 1946: A landslide in the upper forearc?, *Underwater Landslide and Slump Occurrence and Tsunami Hazards off Southern California* (workshop proceedings), Balkema Publishers.

Fukao, Y. (1979). Tsunami earthquakes and subduction processes near deep-sea trenches, J. *Geophys.* Res. 84, 2303-23 14.

Hanks, T. C., and H. Kanamori (1979). A moment magnitude scale, *J. Geuphys. Res.* 84, 2348-2350.

Kanamori, H. (1972). Mechanism of tsunami earthquakes, *Phys. Earth Planet. Interiors 6,* 346-359.

Lander, J. F., and P. A. Lockridge (1989). *United States Tsunamis (including United States possessions) 1690-1988,* National Geophysical Data Center, Publication 4 l-2, Boulder, Colorado.

Pacheco, J. F., and L. R. Sykes (1992). Seismic moment catalog of 1arge, shallow earthquakes, 1900-1989, *Bull, Seismol. Soc. Am.* 82, 1306-1349.

Talandier, J., and E. A. Okal (1989). An algorithm for automated tsunami warning in French Polynesia based on mantle magnitudes, *Bull. Seism. Soc. Am.* 79, 1177-1193.

Walker, D. A. (1992). T-phase spectra, seismic moments, and tsunamigenesis, *Bull. Seis. Soc. Am.* 82, 1275-1305.

Walker, D. A, (1997). *Regional analysis of Ms and Mo values in the Pacific as tsunamigenic indicators for Hawaii,* School of Ocean and Earth Sciences and Technology Report 97-07, Univ. of Hawaii, 54 pp.

Table 1. Pacific-Wide Tsunamis in Hawaii *

Year	Date	Source Locations	Ms	Mw	A (meters)	Location
1819	04 12	Chile	8.5	NA	2.0	W. Coast (B.I.)
1837	1107	Chile	85.	NA	60.	Hilo (B.I.)
1841	0517	Kamchatka	NA	NA	46.	Hilo
1868	08 13	Chile	85.	NA	45.	Hilo
1872	08 23	Aleutians	NA	NA	13.	Hilo
1877	0510	Chile	83.	NA	48.	Hilo
1896	06 15	Japan	76.	NA	55.	Keauhou (B.I.)
1906	01 31	Ecuador	81.	85.	18.	Hilo
1906	08 17	Chile	80.	85.	36.	Maalaea (Maui)
1913	IO 11	N. Guinea	NA	NA	01.	Honolulu
1914	0526	N. Guinea	79.	79.	0.1	Honolulu
1917	05 01	Kermadec	77.	NA	03.	Honolulu
1917	06 26	Samoa	82.	85.	01.	Honolulu
1918	09 07	Kurils	8.0	82.	15.	Hilo
1919	04 30	Tonga	80.	82.	09.	Punaluu (B.I.)
1922	11 11	Chile	81.	NA	21.	Hilo
1923	0203	Kamchatka	81.	85.	61.	Hilo
1923	0413	Kamchatka	70.	70.	03.	Hilo
1927	11 04	California	NA	NA	01.	Hilo
1927	1228	Kamchatka	71.	NA	01.	Hilo
1928	0617	Mexico	76.	77.	02.	Hilo
1929	03 07	Aleutians	73.	78.	02.	Hilo
1931	1003	Solomons	77.	NA	01.	Hilo
1932	06 03	Mexico	80.	79.	04.	Hilo
1932	0618	Mexico	76.	78.	01.	Hilo
1933	03 02	Japan	83.	84.	33.	Kaalualu (B.I.)
1938	11 10	Aleutians	81.	80.	0.3	Hilo
1944	1207	Japan	78.	81.	01	Honolulu
1946	04 01	Aleutians	71.	80.	16.4	Waikolu (Molokai)
1946	1220	Japan	80.	81.	01.	Hilo
1948	09 08	Tonga	76.	NA	01.	Hilo
1949	0822	Canada	81.	80.	01.	Hilo
1950	1005	Costa Rica	77.	NA	01.	Hilo
1950	1023	Guatemala	72.	NA	01.	Hilo
1950	1214	Mexico	71.	72.	01.	Kauai
1952	0304	Japan	83.	81.	03.	Kahului (Maui)
1952	1104	Kamchatka	82.	so.	91.	Kaena (Oahu)
1953	09 14	Fiji	NA	NA	0.1	Kahului
1955	0419	Chile	NA	NA	0.1.	Hilo
1957	03 09	Aleutians	81.	86.	16.1	Haena (Kauai)
1958	0710	Alaska	79.	77.	01.	Hilo
1958	11 06	Kurils	81.	84.	03.	Kahului
1959	0504	Kamchatka	82.	NA	02.	Kahului
1960	0521	Chile	79.	81.	01	Hilo
1960	05 22	Chile	85.		10'7.	Hilo
1960	11 20	Peru	70.	NA	01.	Hilo
1963	10 13	Kurils	81.	85.	04.	Kahului
1963	10 20	Kurils	72.	78.	04.	Kahului
1964	03 28	Alaska	8.4	9.2	4.9	Waimea (Oahu)

Table 1. Pacific-Wide Tsunamis in Hawaii (Continued)

Year	Date	Source Locations	Ms	Mw	A (meters)	Location
1965	**02 04**	**Aleutians**	**8.2**	**8.7**	**1.1**	**N. Coast (Kauai)**
1965	03 30	Aleutians	75 .	76 .	01 .	**Hilo**
1966	10 17	Peru	78 .	81 .	02 .	Kahului
1966	1228	Chile	77 .	77 .	02 .	**Hilo**
1968	**0516**	**Japan**	**81 .**	**82 .**	**05 .**	**Kahului**
1969	08 11	Japan	82 .	82 .	02 .	**Hilo**
1969	11 **22**	Kamchatka	71 .	NA	01 .	Kahuiui
1971	07 **14**	Solomon Is.	78 .	80 .	01 .	Kahului
1971	07 26	Solomon Is.	77 .	81 .	02 .	Kahului
1973	01 30	Mexico	73 .	76 .	01 .	**Hilo**
1973	06 17	Japan	77 .	78 .	01 .	Kahului
1974	**10 03**	**Peru**	76 .	81 .	02 .	Kahului
1976	**01 14**	**Kermadec**	79 .	79 .	01 .	Kahului
1977	**06 22**	**Tonga**	NA	NA	01 .	Kahului
1979	12 12	Ecuador	7.6	82 .	02 .	**Hilo**
1980	07 17	Santa **Cruz** Is.	**7.7**	78 .	01 .	Kahului
1985	03 03	Chile	78 .	80 .	02 .	**Hilo**
1985	09 19	Mexico	81 .	80 .	01 .	**Hilo**
1986	05 07	**Aleutians**	77 .	80 .	06 .	**Kapaa (Kauai)**
1986	1020	**Kermadec**	81 .	79 .	01	**Hilo**
1990	04 05	**Marianas**	75 .	74 .	0'24	**Hilo**
1992	04 25	California	71 .	72 .	**0.15**	Kahului
1992	09 02	Nicaragua	72 .	76 .	0'10	**Hilo**
1993	06 08	Kamchatka	73 .	75 .	**0.12**	**Hilo**
1993	08 08	**Marianas**	80 .	7.7	0'19	Port Allen (Kauai)
1994	**1004**	**Kurils**	**81 .**	83 .	0'48	**Hilo**
1995	07 30	**Chile**	73 .	80 .	0'75	**Hilo**
1995	**1009**	**Mexico**	74 .	80 .	0'37	**Hilo**
1996	06 **10**	**Aleutians**	76 .	79 .	0'55	**Kahului**
1997	**1205**	**Kamchatka**	76 .	77 .	0'60 .	**Kahului**

* Not generated in Hawaii, with reported amplitudes (A) of 0.1 m or more on the main Hawaiian islands and with known source locations along margins of the Pacific. Data through 1899 are taken from Lander and Lockridge (1989). Earthquake data from 1900 through 1989 are taken from Pacheco and Sykes (1992), and from 1990 through 1999 are taken from the U.S. National Earthquake Information Center's (NEIC) monthly listings of earthquakes. Surface wave magnitudes (Ms) are the corrected values in Pacheco and Sykes or the NEIC values after 1989. Through 1989 moment magnitudes (Mw) are based on the preferred moment values (Mo) in Pacheco and Sykes using Mw = [log (Mo) - 9.1] / 1.5 (Hanks and Kanamori, 1979). After 1989 moment magnitudes are based on Harvard solutions in the NEIC bulletins. Earthquakes with an "NA" (not available) entry appearing in the Ms column from 1900 through 1989 are not in the listings of Pacheco and Sykes because their Ms values were believed to be less than 7.0. Earthquakes from 1900 through 1989 with an "NA" entry appearing in the Mw column are those with Mo values in Pacheo and Sykes that are estimated only from tsunami runup data rather than from seismic waves. Pacheco and Sykes also list another 8.5 Ms earthquake at an epicenter nearly identical to that of the 22 May 1960 event. Since both earthquakes occurred within a minute of one another, no distinction can be made in runup heights for those earthquakes and only the largest is listed. Amplitudes through 1987 are runups or tide gauge readings taken from Lander and Lockridge, and from 1988 through 1999 are taken from NEIC monthly listings. There is no consistent method in the original data sources for indicating whether an amplitude was measured on land (i.e., a runup) or was instrumentally recorded (i.e., by a tide gauge). Most, if not all, of the values of a meter or more are probably runups, while values of less than a meter are more likely to be determined from tide gauge readings. Amplitudes listed are only the highest reported values in the main Hawaiian islands (i.e., on either Niihau, Kauai, Oahu, Molokai, Lanai, Maui, or the Big Island). Other values in Hawaii may be found in Lander and Lockridge. To avoid confusion the Island of Hawaii is referred to here by its commonly used alternate name – "the Big Island" (B.I.). Tsunamis reported in Lander and Lockridge as "doubtful", possibly due to air waves, observed, or with only runups of <0.1 m are not listed. Also excluded is a questionable tsunami in 1901 reported in Lander and Lockridge. Reasons for its exclusion are discussed in the text. Data for earthquakes with runups of 0.3 m or more are indicated in bold type.

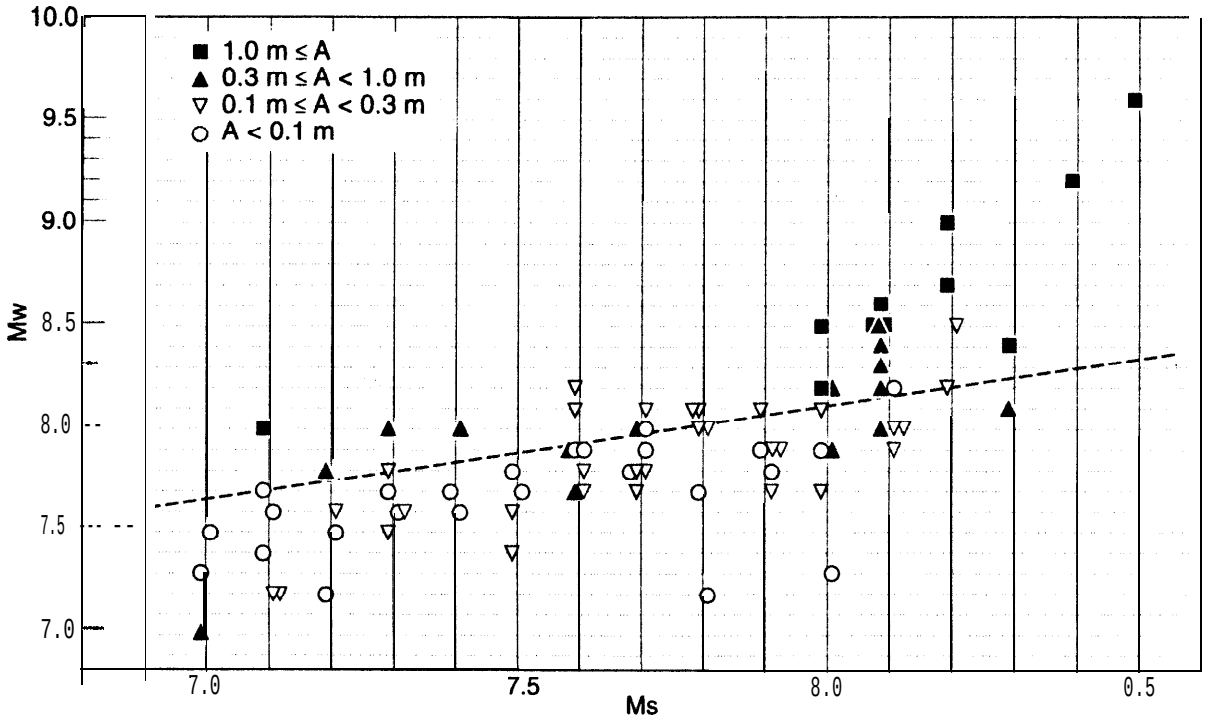

Figure 1. Surface wave magnitudes (Ms), moment magnitudes (Mw), and maximum repotted runups or tide gauge readings (A) in Hawaii from Table I All magnitudes are in tenths of units producing rows (i e., fixed Mw's with varying Ms values) and columns (i e . fixed Ms's with varying Mw values) of data. Surface wave amounts are slightly offset to the left and right of their actual values so as to compare data for "tsunamigenic" and "non-tsunamigenic" regions Values in columns to the left are for earthquakes in the North Pacific and South America The North Pacific is considered to be that portion of the circum-Pacific arc from Alaska at 140 degrees west through Japan and the Marianas. Values in columns to the right are for the South Pacific (i e., the circum-Pacific arc from New Guinea through New Zealand), Central America. and North America to 140 degrees west Of the more than 200 earthquakes examined for these regions, most did not generate reported tsunamis in Hawaii or their tsunamis were reported either to be less than 0 l m or to be "observed". Such events are not listed in Table 2, but the largest of these in terms of Mw for each Ms value are plotted in this figure Additional discussions may be found in the text,

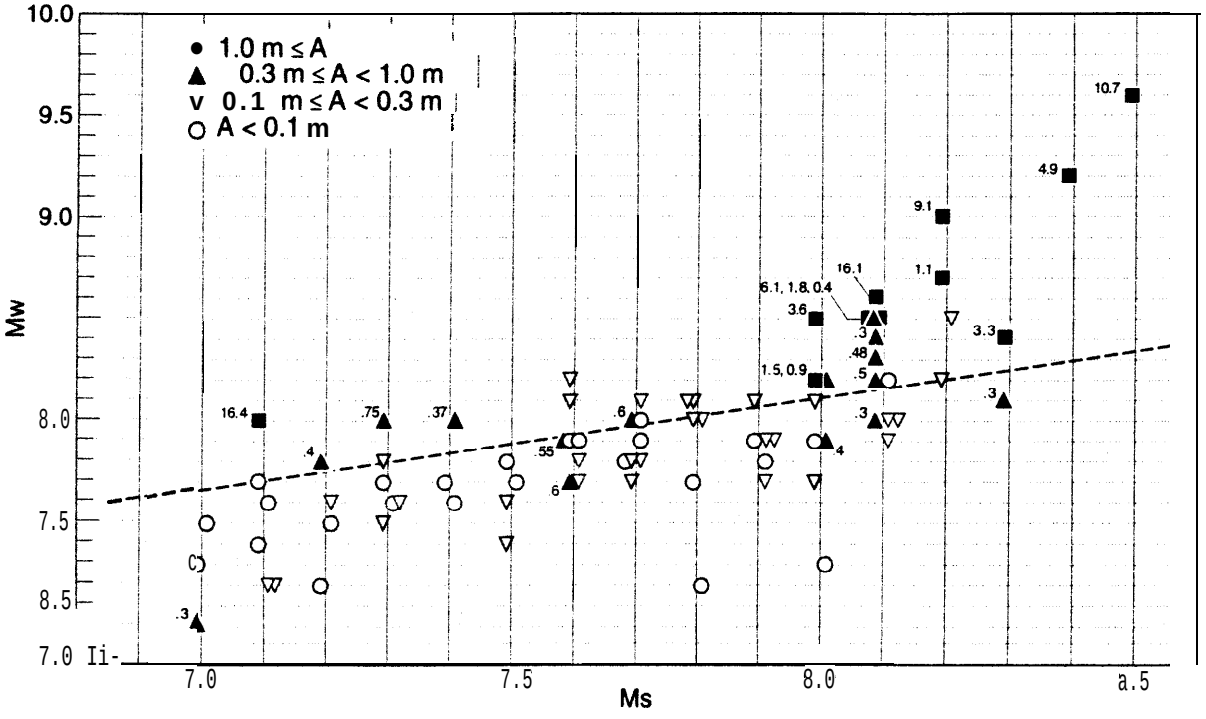

Figure 2. Runup values of 0 3m or more indicated for the data points of Figure 1.

s oURCE SIMULATION FOR TSUNAMIS: LESSONS LEARNED FROM FAULT RUPTURE MODELING OF THE CASCADIA SUBDUCTION ZONE, NORTH AMERICA

George R. Priest
Oregon Department of Geology and Mineral Industries, 313 SW 2nd, Suite D, Newport, Oregon 97365

Edward Myers and António M. Baptista
Oregon Graduate Institute of Science & Technology, P.O. Box 91000, Portland, Oregon 97291-1000

Paul Fleuck and Kelin Wang
Geological Survey of Canada, Pacific Geoscience Centre, Sidney, BC, V8L 4B2, Canada

Curt D. Peterson
Portland State University, PO Box 751, Portland, Oregon, 97207

ABSTRACT

Fault rupture simulations of great subduction zone earthquakes on the Cascadia subduction zone are explored utilizing standard algorithms of Okada (1985) applied to simplified geologic models in order to provide the sea floor deformation for tsunami simulations. Findings from this exercise include: (1) the Okada (1985) algorithm produces anomalous "spikes" of uplift exceeding the predicted geometric uplift at the up-dip tip of thrust fault ruptures; (2) simulated thrust fault ruptures should therefore be extended to (or very near) the surface to minimize this source of error; (3) because of the "spike" effect, variations in slip across an accretionary wedge (seaward transition zone) is best simulated by a series of individual ruptures, each reaching the surface, rather than by progressive changes in slip on a single rupture coinciding with the plate interface; (4) paleoseismic data from estuarine marshes and coastal geodetic information can constrain total slip, width, and length of megathrust ruptures but not offshore deformation; (5) while still highly uncertain, paleoseismic data is permissive of slip on the order of 15-20 m, rupture length of 1000 km, and minimum rupture width of 140 km; (6) likely presence of asperities and splay faults that partition significant slip is a very large source of error; and (7) total potential coseismic slip is highly speculative, owing to uncertainties in aseismic slip, amount of main shock versus after shock slip, potential post-seismic subsidence, and oblique convergence partitioned to lateral faults in the North American Plate. Submarine landslides are an additional source of tsunami excitation not treated in this investigation. Characterization of tsunami sources is best addressed by an inter-disciplinary approach that incorporates geological, geophysical, and numerical modeling expertise.

INTRODUCTION

Scientific findings of the last several years have shown that the Washington, Oregon, and northern California coast is vulnerable to great (M 8-9) earthquakes that can occur on the offshore Cascadia subduction zone fault system (Figures 1 and 2; Atwater and others, 1995, Nelson and others, 1995; Clague, 1997). Such earthquakes can generate tsunamis that will be hazardous to populated areas of the Pacific Northwest coast (e.g. see previous investigations of (Hebenstreit and Murty, 1989; Whitmore 1993; 1994; and Priest, 1995). This study explores possible fault dislocation scenarios for great earthquakes on the Cascadia subduction zone. These scenarios provided the sea floor deformation for a companion study of numerical simulations of tsunami inundation (Myers and others, 1999). The investigation illuminated a number of uncertainties in the complex source modeling process that should be taken into account when interpreting tsunami simulations. Figure 2 schematically illustrates possible fault rupture complexities in the subduction zone and geological terms used to describe the rupture process.

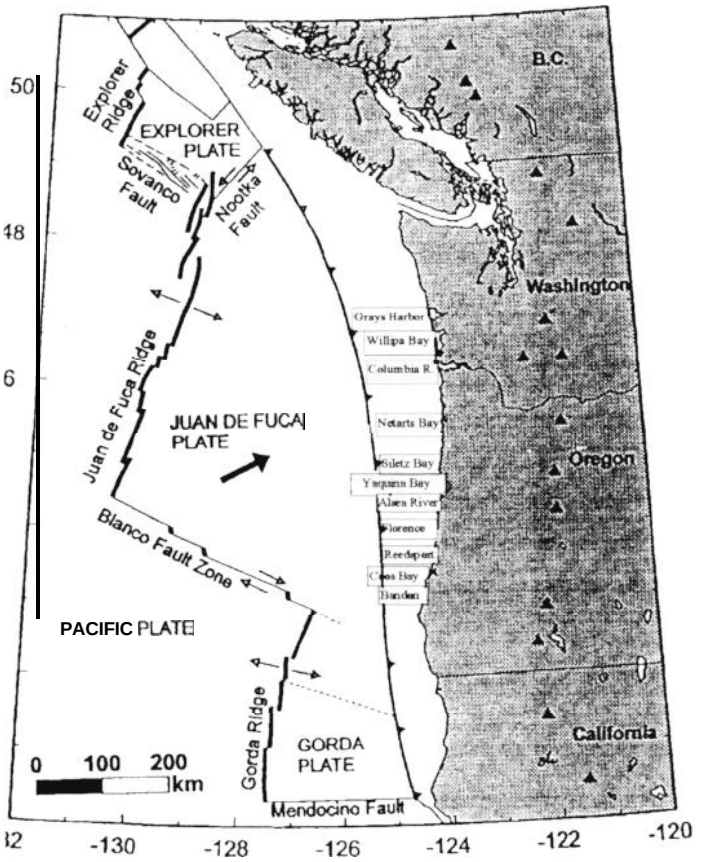

Figure 1. Plate tectonic map of the Cascadia subduction zone fault system illustrating the location of the surface trace of the fault at the deformation front (toothed pattern) and localities mentioned in the text. The subduction zone is bounded by the Nootka and Mendocino transform faults and dips 8-12° toward the east. Figure modified from Fleuck and others (1997).

Fleuck and others (1997) tested the three-dimensional model and found that it reproduced surface deformations from Okada's (1985) three-dimensional rectangular solution and Savage's (1983) two-dimensional solution. The best fits were obtained by descretizing the calculation to sufficient triangular elements to reproduce a smooth pattern of displacement.

The computational domains for this study cover the entire region of the Cascadia subduction zone south of the Nootka Fault at Vancouver Island and north of the Mendocino Fracture Zone (Figure 1), extending on land far enough to cover the full extent of each fault rupture. The grids are arranged in triangular elements whose size is smaller where the model must simulate sharp transitions in slip or dip.

CASCADIA FAULT RUPTURE PARAMETERS

Rupture Length

The most completely studied Cascadia earthquake is the one that occurred about 300 years ago (e.g. Atwater and others, 1995). Historical and paleoseismic data support a moment magnitude of 9 and rupture length approaching 1,000 km, the full length of the subduction zone. Nelson and others (1995) argue that the most reasonable earthquake scenario that could explain paleoseismic data for this earthquake is a single rupture that encompassed most of the length of the subduction zone. A series of smaller earthquakes are also consistent with the data, but they would have had to occur within a period of less than 20 years to explain the dendrochronologic ages of trees killed by coseismic subsidence (Nelson and others, 1995). World wide analogues for multiple ruptures on this time frame are rare (Nelson and others, 1995) and there is no paleoseismic evidence to support this scenario. Unless the ruptures occurred over periods of a year or less, multiple tsunamis so generated would leave stratigraphic records of sand layers with intervening intertidal mud layers, but such records are rare in local paleoseismic data, even in areas with rapid estuarine sedimentation (Darienzo and Peterson, 1995; Peterson and Darienzo, 1996). Instead, most candidate tsunami deposits, particularly those thought to correlate with the 1700 AD event, are single thin blankets of sand with negligible intertidal mud interbeds (Atwater, 1992; Peterson and Darienzo, 1996; Clague and Bobrowsky, 1994; Darienzo and others, 1994; Darienzo and Peterson, 1995; Peterson and Priest, 1995; Peterson and others, 1997).

Satake and others (1996) concluded from study of historical records in Japan that a destructive tsunami striking the Japanese coast in 1700 AD is consistent with a magnitude 9 Cascadia subduction zone earthquake that ruptured most of the subduction zone. Uncertainties in the numerical simulation of Satake and others (1996), however, make the magnitude assignment highly speculative, and sources other than Cascadia are not ruled out. The match of this date to the dendrochronologic data of Nelson and others (1995) is, however, permissive evidence of a Cascadia event.

All subduction zones appear to rupture more or less randomly within and across various segment boundaries (e.g. Ando, 1975; Huang and Turcotte, 1990), so a segmented rupture may possibly occur at Cascadia in the future. Geomatrix (1995) assigned the highest probability to a maximum rupture length of 450 km, based on a statistical analysis of aspect ratios of large (magnitude >7.0)

thrust earthquakes and potential geological segment boundaries. Goldfinger and others (1992a; 1992b; 1993; 1994) argue that ruptures on Cascadia should be 600 km or less in length because of the narrow locked width, heterogeneous uplift rates onshore, the broad, weak accretionary wedge, and total lack of seismicity in the wedge. McCaffrey and Goldfinger (1995) concluded that Cascadia has a weak deforming upper plate similar to subduction zones world wide that lack great (magnitude 9) earthquakes.

We conclude that the simulations need to examine both full-length and segmented ruptures to cover uncertainties. A rupture length of 1,050 km, extending from the Nootka Fault to the Mendocino Fracture Zone, will cover the maximum rupture case. A rupture length of 450 km, the most probable length from the Geomatrix (1995) engineering analysis, will be used for the segment break scenario. Two segment ruptures will be considered., one propagating 450 km north to southern Vancouver Island and one propagating south to Eureka, California from a centrally located latitude of 44.8° N.

Rupture Dip

Rupture dip is assumed to correspond to the dip of the decollement on the Cascadia subduction zone. The decollement is thought to lie near the top of the subducted oceanic plate throughout much of the margin (Davis and Hyndman, 1989; Hyndman and others, 1990; and Hyndman and Wang, 1993). The geometry of the decollement below a depth of about 5 km is taken from Fleuck and others (1997) who refined the geometry of Hyndman and Wang (1995) utilizing Benioff-Wadati seismicity, seismic reflection, seismic refraction, teleseismic wave form analysis, and seismic tomography. Their structure contours on the top of the slab, referenced to mean sea level, are shown in Figure 3. The vertical positional error on the contours is estimated to ±0.5 km for the seaward end, increasing to ±5 km at depths of 50 km. The decollement dips 8-12° in potentially seismogenic parts of the subduction zone. The actual model fault plane was smoothed through the data of Fleuck and others (1997) utilizing a polynomial function.

The seaward 2-5 km of the simulated fault plane is extrapolated from the top of the subducted slab to the surface trace of the deformation front utilizing a polynomial curve. The thick (2-3 km) cover of sediment on the subducting slab makes this extrapolation necessary.

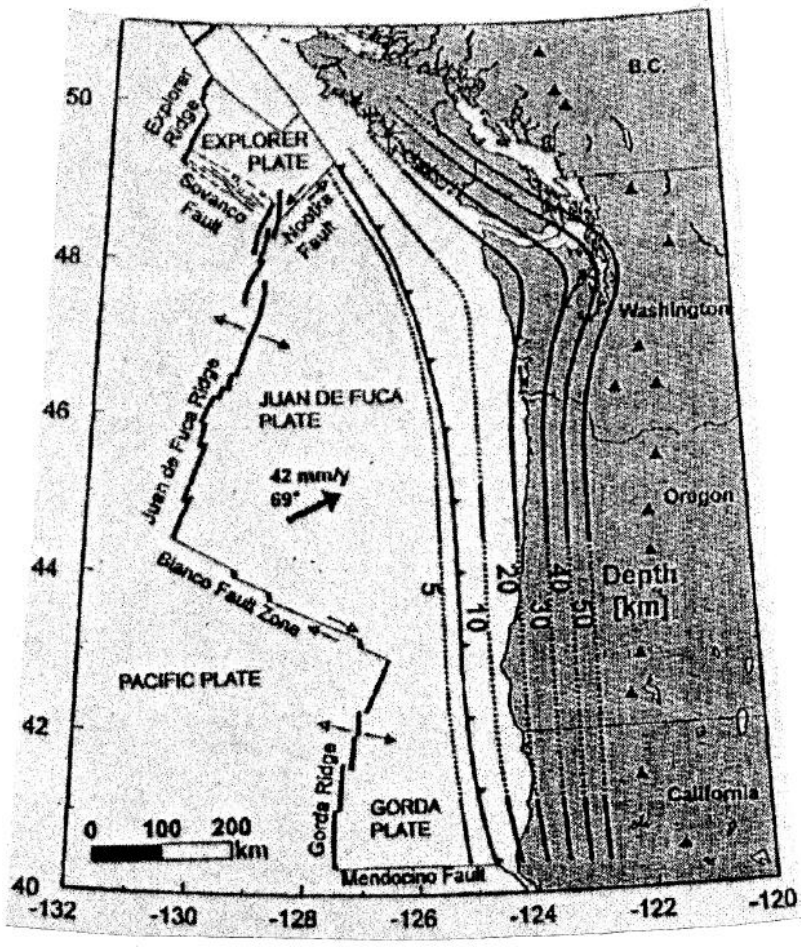

Figure 3. Strike and. dip of the subduction zone. Structure contours are in kilometers referenced to sea level. Figure taken from Fleuck and others (1997).

Slip

Rogers (1988; his Table 2) showed that if the recurrence rate for Cascadia earthquakes is on the order of 466 years for a single rupture encompassing the Juan de Fuca-Gorda plates (1000 km), the ratio of seismic slip to total convergence slip would be on the order of 1.0 (no aseismic slip). This is close to the mean Cascadia recurrence of 400-500 years estimated independently from paleoseismic data (Geomatrix, 1995; Darienzo and Peterson, 1995; Atwater and Hemphill-Haley, 1996).

While it is recognized that a coupling ratio near 1.0 is questionable from a theoretical point of view (e.g.. Kanamori, 1977), it will be used here to establish an upper limit for coseismic deformation and associated tsunami generation. As explained below, a coupling ratio of about 0.5 will in effect be emulated by the segment rupture scenarios, since they will have about half the slip of the scenario 1,050 km rupture.

Coseismic slip was calculated by multiplying the convergence rate by recurrence. The rate and direction of convergence of the Gorda and North American Plate is not known with certainty, owing to probable internal deformation of the Gorda Plate, but the rate of convergence probably follows the southerly decreasing pattern apparent in the data for the Juan de Fuca Plate (e.g. Riddihough, 1984). Hence, all slip calculations are based on the Euler pole solution for Juan de Fuca-North American Plate motion from DeMets and others (1990). Convergence direction varies from N69°E to N59°E and convergence rate from 44 to 34 mm/yr from north to south.

McCaffrey and Goldfinger (1995) argue that nearly all of the strike-parallel component of oblique convergence is taken up by inelastic deformation in the North American Plate. The hypothesis is that the strike-parallel component drives clockwise rotation of large blocks of the upper plate. Goldfinger and others (1992a; 1992b; 1993) mapped 9 west northwest trending left lateral faults bounding these blocks on the continental slope from the latitude of Cape Blanco, Oregon (43° N) to Grays Harbor, Washington (47° N). This inelastic deformation could reduce the interseismic slip deficit on locked and partially locked portions of the subduction zone by as much as 13 percent in this portion of the margin. This potential reduction in slip is not simulated here, so simulated deformation in the central and southern part of the Cascadia margin may be 13 percent too high, if this hypothesis is correct.

Assuming a coupling ratio of 1.0, mean recurrence of 450 years (Geomatrix, 1995), and rupture length of 1,050 km, coseisrnic slip will be on the order of 15-20 m with a slip-rupture length ratio of 1.4-1.9 x 10^{-5}. This ratio is similar to the 2 X 10^{-5} ratio thought by Scholz (1982)to characterize subduction zone ruptures world wide.

Using this same 15-20 m slip for the scenario segment ruptures of 450 km length yields slip-length ratios of 3-4 X 10^{-5}, much larger than the 2 X 10^{-5} ratio of Scholz (1982). Slip should be about 9 m for such a short segment rupture, if the Scholz (1982) ratio holds. This amount of slip demands a recurrence between of 205 and 265 years for the convergence rates used here. Assuming mean convergence at about 40 mm/yr, a mean recurrence of 225 years is appropriate for calculation of slip for the two segmentation scenarios. The slip so calculated effectively emulates a coupling ratio of about 0.5 for the known recurrence of 450 years, even though it does so utilizing two segment breaks instead of one long rupture.

Coseismic slip at the locked zone may decrease up and down dip from the fully locked fault interface (e.g. see discussions by Hyndman and Wang, 1993;1995). The distribution of slip in these landward and seaward transition zones is best understood in the context of rupture width.

Rupture Width and Sip Distribution

The Cascadia subduction zone is one of a class of subduction zones where young (<20 Ma) oceanic crust is subducting. The width of the rupture in analogous subduction zones world wide is on the order of 100 km (Rogers, 1988). Hyndman and Wang (1995) proposed that rupture width is determined by the 450° C isotherm which marks the point where stick-slip changes to stable sliding. The fault interface between 350° C and 450° C would then mark a transitional area termed the landward transition zone (LTZ) between a fully locked condition and stable sliding. The lateral uncertainty in the down dip position of these isotherms is on the order of ±20 km for

portions of the subduction zone where the dip profile is well constrained (Hyndman and Wang, 1995). The uncertainty is larger where the profile is less well known, as in central Oregon and northern California, but the amount of uncertainty there was not specified explicitly by Hyndman and Wang (1995). This high degree of uncertainty is probably why there is some mismatch between interpretations of rupture width in central and northern Oregon from paleoseismic data versus geophysical data of Hyndman and Wang (1995) and Fleuck and others (1997). Positions of the 350° C and 450° C isotherms from Fleuck and others (1997) will be used for one rupture scenario (Scenario 1, Figure 4).

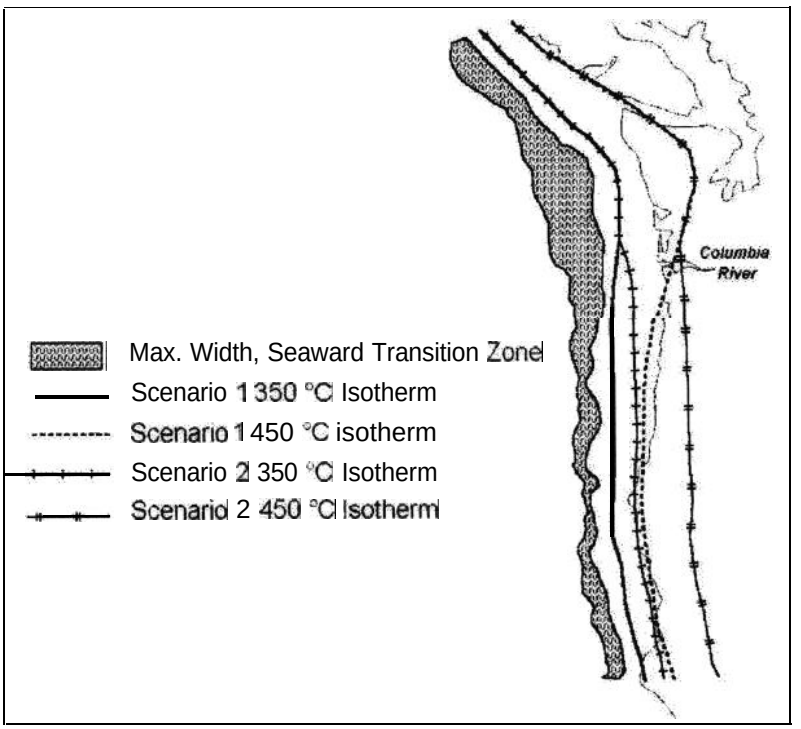

Figure 4. Location of isotherms and maximum width of seaward transition zone on the Cascadia subduction zone. Isotherms for Scenario 1 are from Fleuck and others (1997). Isotherms for Scenario 2 are the same as Fleuck and other (1997) north of the Columbia River,.but south of the river they extend further east.

In an earlier study Priest (1995) found that a match to paleoseismic data in northern and central Oregon could be achieved by locating the 350 °C isotherm approximately 70 km down dip from the deformation front with the 450° C isotherm another 70 km down dip (140 km-wide rupture). This 70+70 model will be used here to explore the possible effects of a wide rupture on tsunami propagation in Oregon and northern California. The 70+70 model uses the Fleuck and others (1997) location of isotherms in Washington and the Columbia River but the 70+70 assumption to the south (Scenario 2, Figure 4). The results will then be compared to paleoseismic data of Peterson and others (1997) which estimates the amount of coseismic subsidence from interpretations of buried estuarine soils. See Atwater (1992), Atwater and Hemphill-Haley

(1996), Peterson and Darienzo (1996), and Peterson and others (1997) for summaries of how buried marsh soils can be used to infer coastal subsidence.

Coseismic rupture penetration through the accretionary wedge is largely unknown. Figure 2 shows one possibility, based on known structures in the wedge. This complex behavior is difficult to simulate with simple models. Simulations here will assume that a seaward transition zone (STZ) exists that corresponds to where coupling between the two plates becomes weak. An interpretation of the maximum landward boundary of the STZ is given in Figure 4; this corresponds chiefly to the slope break at the top of the continental slope. This boundary is also where many fold axes rotate from parallel to the margin to perpendicular to the convergence direction. Even though coupling may be weak in the STZ, it is possible that ruptures can still penetrate through it as the upper plate "pushes from behind" during elastic strain release. A perspective view of the relationship of the STZ to isotherms and the fault interface is given in Figure 5.

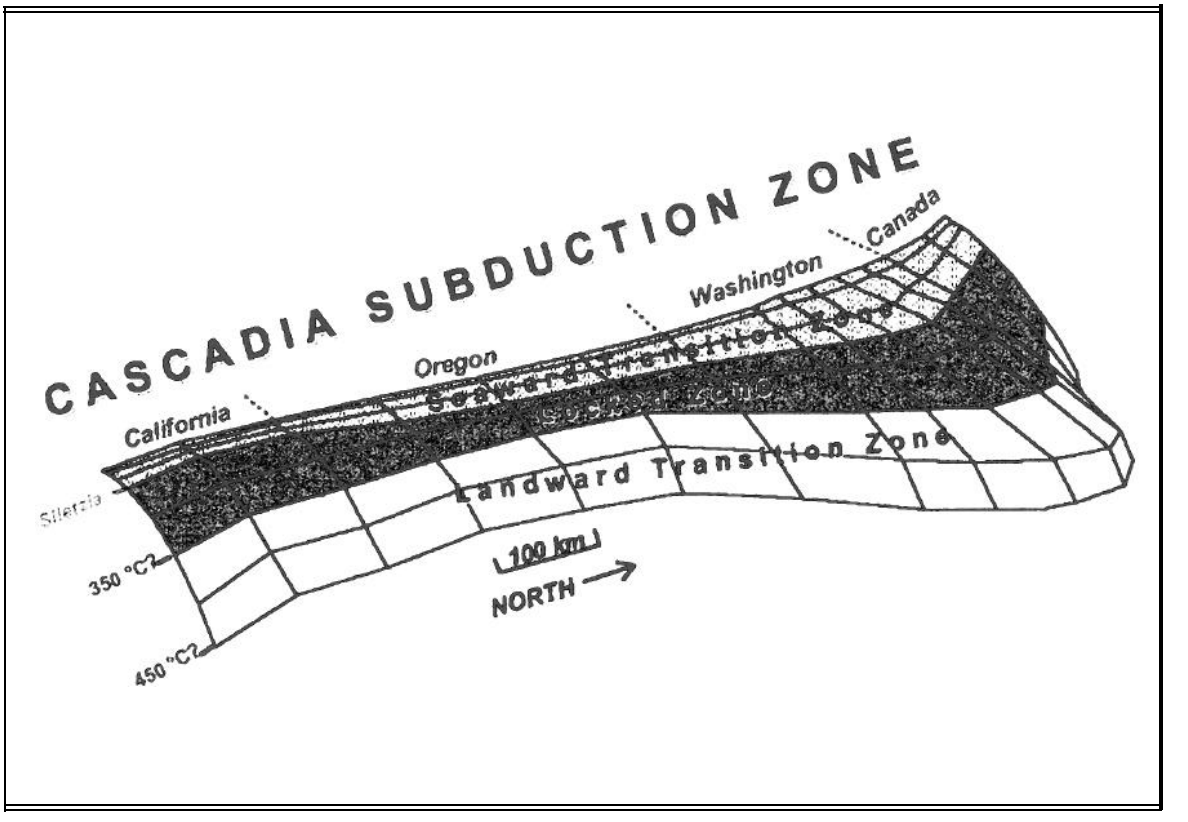

Figure 5. Perspective view of the plate interface on the Cascadia subduction zone illustrating schematically the seaward transition zone (STZ), locked zone (LZ), and landward transition zone (LTZ) relative to isotherms. Siletzia refers to the up dip contact of the Siletz River Volcanics with sedimentary rocks of the accretionary wedge. Figure modified from Fleuck and others (1997).

To test all possibilities from no rupture penetration of the STZ to essentially full penetration, three scenarios will be explored:

1. ***Scenario*** A: Slip equal to that of the LZ for all but a narrow (2-5 km) zone at the deformation front where slip decreases linearly to zero.
2. ***Scenario B:*** Linear decrease in slip across the maximum potential width of the STZ.
3. ***Scenario C:*** Essentially no slip in the STZ. This will be achieved by linearly decreasing slip to zero over a narrow (2-5 km) zone at the landward boundary of the STZ.

These three slip distributions are summarized schematically in Figure 6.

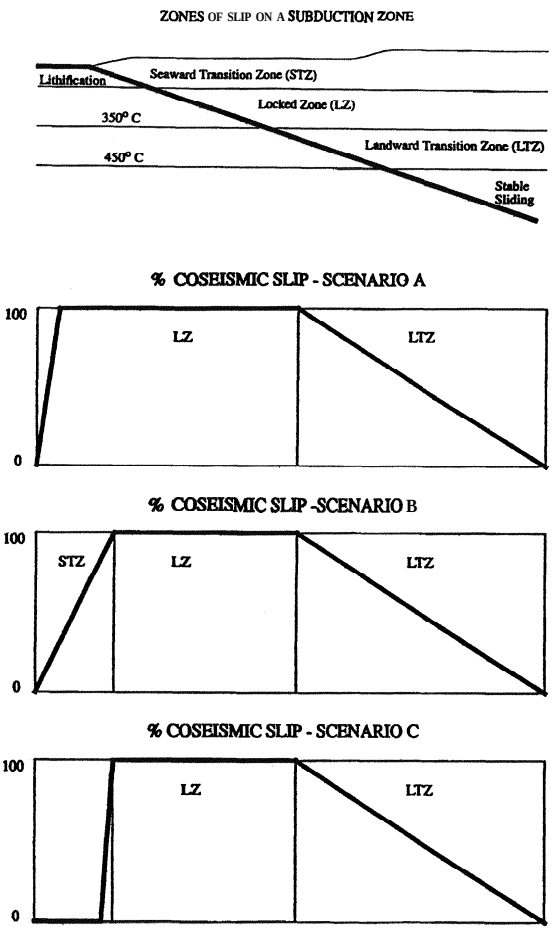

Figure 6. Schematic of three simple slip distributions utilized for simulation of fault rupture. All share the same linear slip in the landward transition zone. Scenario A assumes full coseismic slip through most of the seaward transition zone (STZ); Scenario B assumes linear decrease in slip; and Scenario C assumes negligible rupture penetration of the STZ.

CASCADIA RUPTURE SCENARIOS

Cascadia subduction zone scenarios for various rupture widths and slip distributions are summarized in Table 1 for ruptures 1050 km long. For segment break scenarios, only two will be considered. These are summarized in Table 2. Crude estimates of moment magnitude are given in Table 3.

Table 1. Scenarios assuming a 1,050 km rupture length, but varying widths. Rupture scenarios are based on two rupture widths (Figure 4) and the three seaward transition zone (STZ) coseismic slip distributions (Figure 6). All assume strain accumulation at 100 percent of the convergence rate over 450 years and a linear change in coseismic slip in the landward transition zone (LTZ). The locked zone and LTZ of Scenario 1 is narrower than Scenario 2 in Oregon and northern California (Figure 4).

Seaward Transition Zone (STZ) Slip Distribution (STZ is 15-60 km wide, being wider in the northern part of the Cascadia margin)	SCENARIO 1 1,050 km-long rupture of Fleuck and others (1997); (~70 km wide in Oregon and northern California)	SCENARIO 2 1,050 km-long rupture, matching Fleuck and others (1997) in Washington but ~140 km wide in Oregon and northern California
SCENARIO A (linear decrease in slip east to west in a 2-5 km wide zone at westward edge of the STZ)	Model 1A	Model 2A
SCENARIO B (linear decrease in slip east to west across the entire STZ;)	Model 1B	Model 2B
SCENARIO C (linear decrease in slip to 0 across a 2-5 km zone at the eastern edge of the STZ)	Model 1C	Model 2C

Table 2. Segment break scenarios, assuming segmented ruptures. Scenarios are created by calculating slip from a 225 year recurrence (or coupling ratio of 0.5 for 450 years recurrence) and assuming the slip distribution and rupture width of Model 2C (Table 1).

Slip Distribution and rupture width of Model 2C	North Segment Rupture extends 450 km north from 44.8° N latitude	South Segment Rupture extends 450 km south from 44.8° N latitude
~140 km wide rupture in Oregon and northern California; 15-60 km STZ; zero slip in all but easternmost 2-5 km of STZ	Model 2Cn	Model 2Cs

Table 3. Earthquake magnitude parameters for each scenario. Calculations of moment magnitude assume rigidity = 4 x 10^{11} dyne/cm^2. Note that these magnitudes are upper limits, since they assume, as does the elastic model of Okada (1985), that slip in the STZ (accretionary wedge) is entirely from stick-slip behavior, rather than rupture penetration into relatively weak rock with high fluid pressures, as is likely the case.

Scenario	Rupture Length (km)	Locked Width (km)	Locked Width in. Partially Locked zones (km)	Weighted Mean Locked Width (km)	Slip (m)	(M_w)
1A	1,050	35-105	20-58	78	15-20	9.1
1B	1,050	14-43	33-88	64	15-20	9.0
1C	1,050	14-43	20-58	51	15-20	9.0
2A	1,050	60-105	38-58	107	15-20	9.2
2B	1,050	29-50	48-88	92	15-20	9.2
2C	1,050	29-50	38-58	79	15-20	9.1
2Cn	450	29-43	38-58	80	7-10	8.7
2Cs	450	43-50	38	77	7	8.6

In addition to these Cascadia scenarios, a number of generalized simulations were done by Fleuck (1996) to explore how the Okada (1985) point source model affected deformation. These findings will be summarized before examining the Cascadia scenarios.

RESULTS

Sensitivity Analysis for Variations in Vertical Deformation

Utilizing the same rupture simulation technique as this study, Fleuck(1996) performed sensitivity analysis for variations surface deformation in response to changes in thrust fault width, dip, depth, displacement, and transitions between full and partial slip. He found that the fault parameters generally follow simple geometric predictions. Simple geometry demands that decreasing the vertical component of displacement, by decreasing dip or slip, decreases vertical deformation. Deeper burial of the rupture produces smaller, broader surface deformation (Figure 7). Likewise, increasing the width of the rupture broadens the zone of coseismic uplift and subsidence but without significant decrease in vertical displacement for a given slip (Figure 8). The trough of maximum subsidence over a fully locked rupture lies approximately above the down dip end of the rupture (Figures 7 and 8).

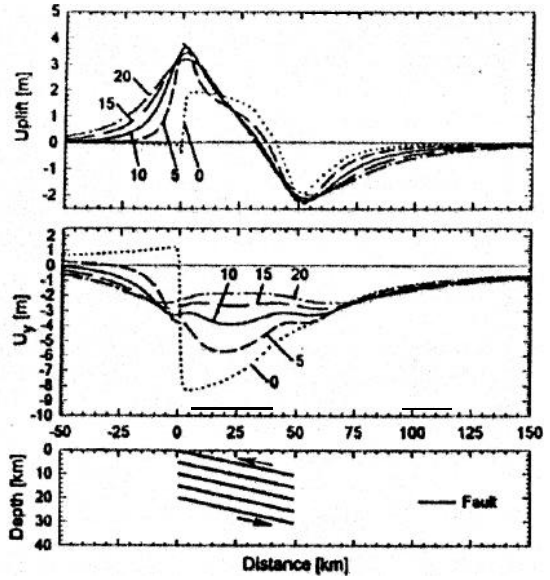

Figure 7. Sensitivity of surface defarmation to burial of a rupture 1000 km long and 50 km wide with 10 m of pure dip slip thrust motion and dip of 12 degrees. Horizontal (U) and vertical deformation are illustrated, Note how deformation decreases with burial from 0 to 20 km. Maximum geometric uplift for the fault is shown for the 0 km case. Note the anomalous "spikes" of uplift at the up dip ends of buried ruptures (Figure taken from Fleuck, 1996).

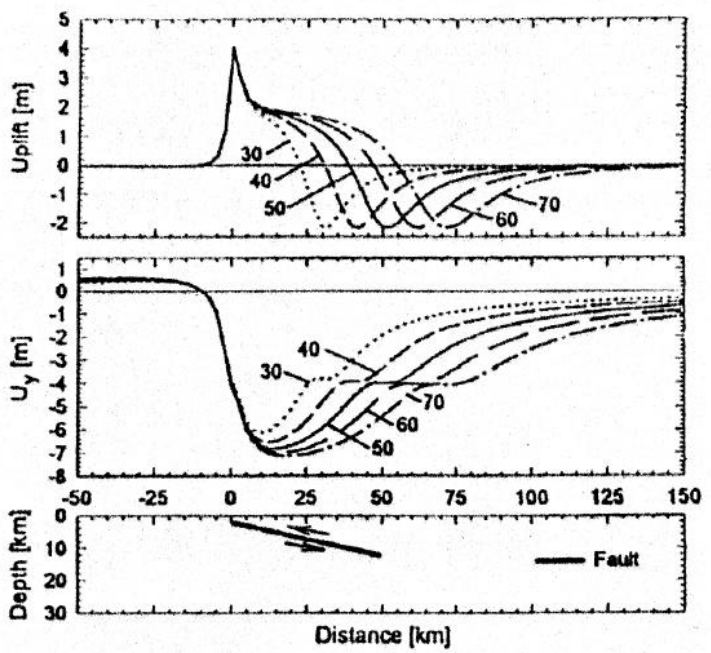

Figure 8. Sensitivity of surface deformation to rupture width on a fault 1000 km long with a slip of 10 m and dip of 12 degrees. Numbers are widths in kilometers. Note that if this were a subductian zone rupture, the trough of subsidence migrates landward with increasing width but maintains the same depth, Down dip tips of ruptures are at the point of maximum coseismic subsidence (Figure taken from Fleuck, 1996).

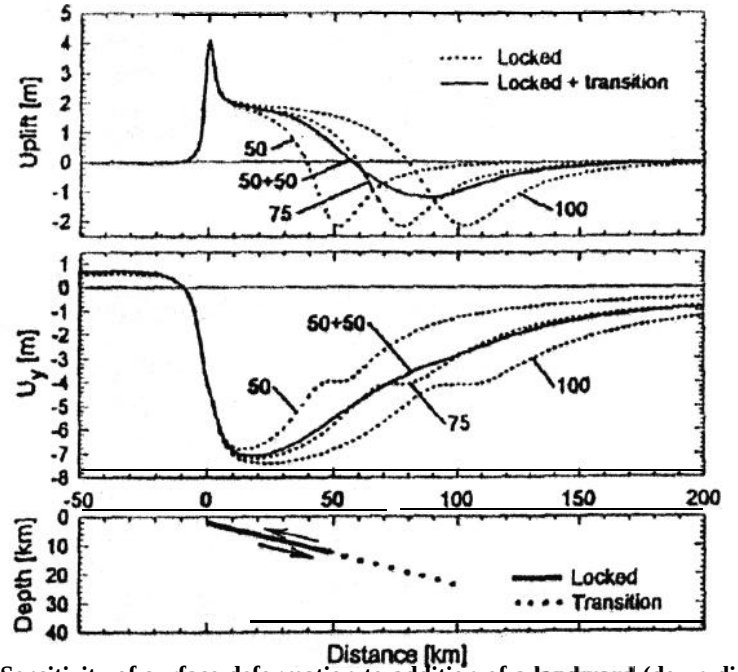

Figure 9. Sensitivity of surface deformation to addition of a landward (down dip) transition zone (LTZ). The fault is 1000 km long with dip of 12 degrees and 10 m of pure dip slip thrust motion. The locked and transition zones are SO km wide. Slip decreases linearly from 10 m to zero in the transition zone. Coseismic deformation from fully locked buried ruptures with widths of 50, 75, and 100 km are shown for comparison, Note how the SO + 50 rupture produces about half as much subsidence as the fully locked 75 km rupture even though both have the same total slip and same location of maximum subsidence. Simulation of paleoseismic subsidence without a LTZ would lead to estimates of total slip that are too small (Figure taken from Fleuck, 1996).

The effect of adding a landward transition zone, decreasing linearly from full slip to zero slip in down dip direction is illustrated in Figure 9. Uplift and horizontal deformation are shown for a fault with 50 km locked and 50 km transition, compared to fully locked zones with widths of 50, 75, and 100 km. Variations in the landward transition zone do not influence the deformation pattern near the up dip end of the fault, and, for a given net slip, there is less but broader coseismic subsidence with a transition zone than without. The former observation shows that paleoseismic estimates of coastal subsidence in estuaries tell one nothing about offshore deformation patterns. The latter observation shows that it will take more slip to match a given estimate of paleoseismic subsidence with a landward transition zone than without. The 75 km fully locked and 50+50 case in Figure 9 illustrate this latter point. Even though both produce the same lateral position for the trough of maximum subsidence (because both have the same total seismic slip), the 75 km locked zone has about twice the subsidence of the 50 + 50 km case; hence the distribution of slip and width of the LTZ are critical to interpretation of paleo-deformation data.

When a thrust fault rupture is buried, the model generates a "spike" of anomalous uplift at the up dip end of the rupture (Figures 7-9). This spike disappears when the fault slips all the way to the surface (Figure 7,0 km case). Allowing the rupture to reach the surface limits uplift to the 2 m geometric uplift for a fault dipping 12°. In contrast, buried ruptures produce spikes nearly twice the geometric uplift (Figure 7). The effect of a spike on tsunami generation is minimal, if it is

narrow, as when the rupture reaches nearly to the surface. Priest (1995) found that an uplift spike added only about 3 percent to the run-up elevation on Cascadia subduction zone scenarios where slip on the megathrust was decreased linearly to zero within about 0.7 km of the surface over a lateral distance of 5 km.

Cascadia Scenario Ruptures

Figures 10-17 show map views of vertical deformation for all of the fault dislocation models of Tables 1 and 2; Figure 18 illustrates cross sectional views in central Oregon at the latitude of Yaquina Bay (Newport). The most striking diierence in the scenarios is the extremely narrow width of the locked zone and attendant uplift for Scenario 1 relative to Scenario 2, especially when slip in the seaward transition zone is removed (e.g. Model 1C, Figures 12 and 18). The other big difference is the onshore trough of subsidence in Scenario 2 (Models 2A-2C) versus the offshore trough predicted by Scenario 1 (Models 1 A-1C) from the Columbia River south. The onshore trough of subsidence in Scenario 2 (Models 2A-C) was designed to roughly match paleoseismic data indicative of increasing subsidence landward of the coast in Oregon (Figure 19; Peterson and others, 1997).

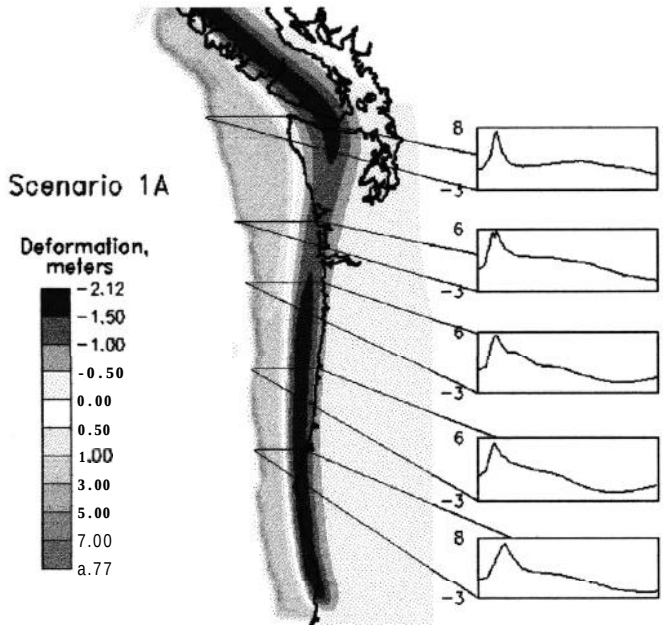

Figure 10. Map of coseismic deformation for Model 1A (labeled Scenario 1A in this figure from Myers and others, 1999).

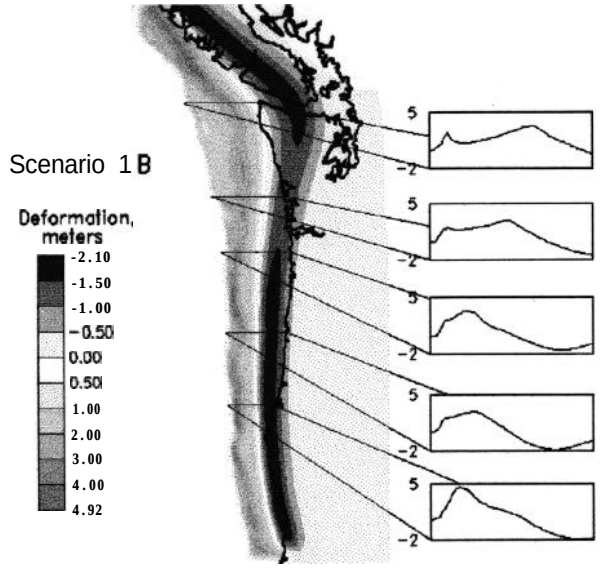

Figure 11. Map of coseismic deformation for Model 1B (labeled Scenario 1B in this figure from Myers and others, 1999).

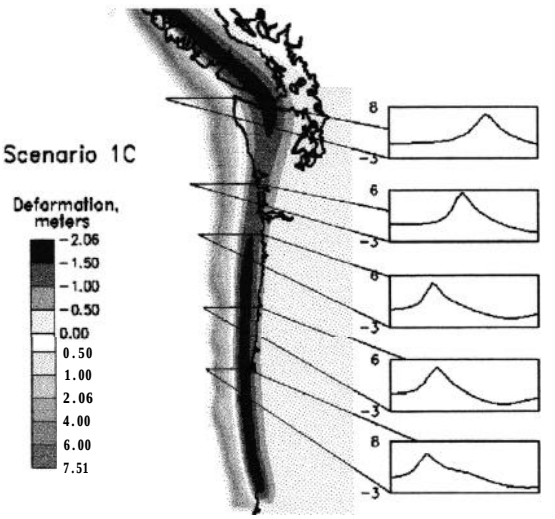

Figure 12. Map of coseismic deformation for Model 1C (labeled Scenario 1C in this figure from Myers and others, 1999).

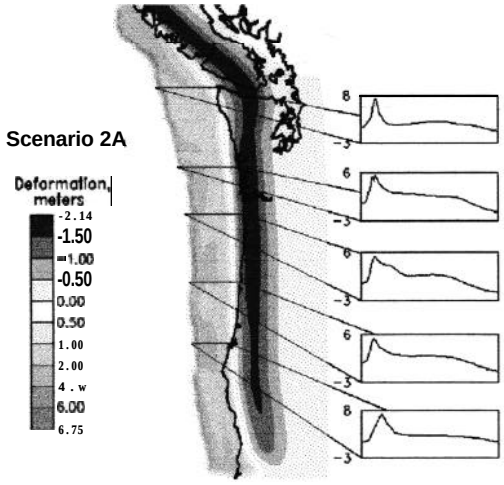

Figure 13. Map of coseismic deformation for Model 2A (labeled Scenario 2A in this figure from Myers and others, 1999).

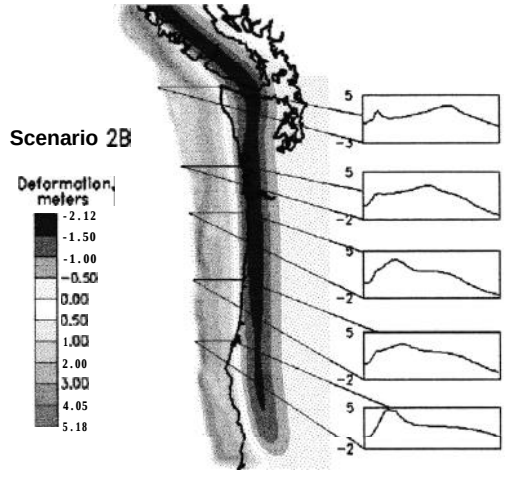

Figure 14. Map of coseismic deformation for Model 2B (labeled Scenario 2B in this figure from Myers and others, 1999).

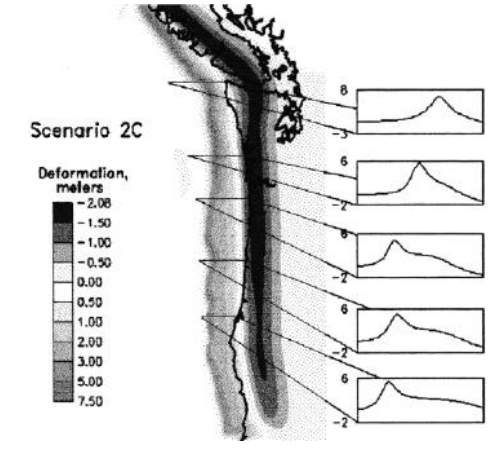

Figure 15. Map of coseismic deformation for Model 2C (labeled Scenario 2C in this figure from Myers and others, 1999).

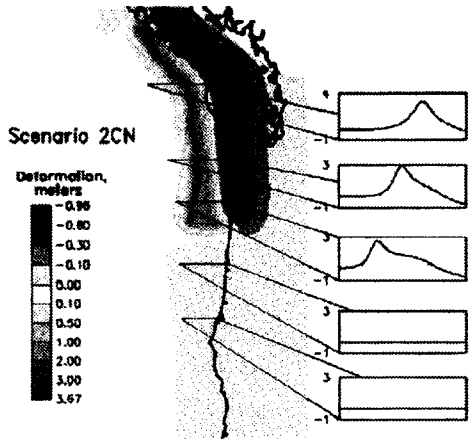

Figure 16. Map of coseismic deformation for Model 2Cn (labeled Scenario 2Cn in this figure from Myers and others, 1999).

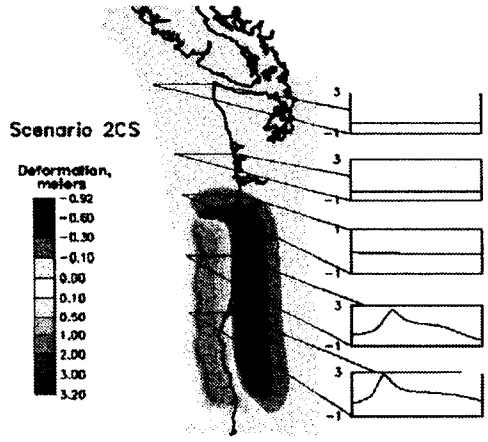

Figure 17. Map of coseismic deformation for Model 2Cs (labeled Scenario 2Cs in this figure from Myers and others, 1999).

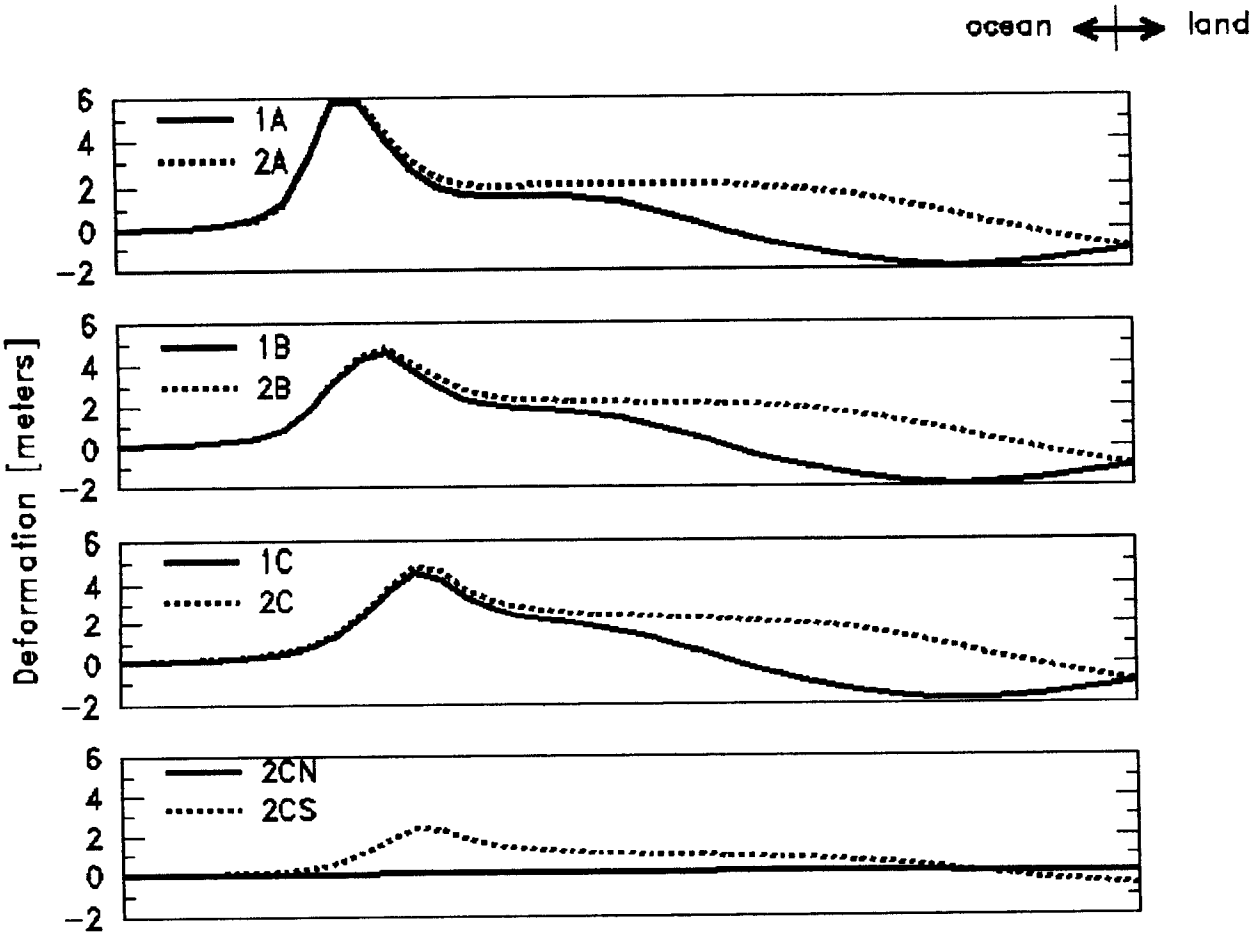

Figure 18. Cross sections of simulated coseismic deformations at the latitude of Yaquina Bay on the central Oregon coast (see Figure 1 for location). Figure is from Myers and others (1999) and shows only those models utilized by them for tsunami simulations.

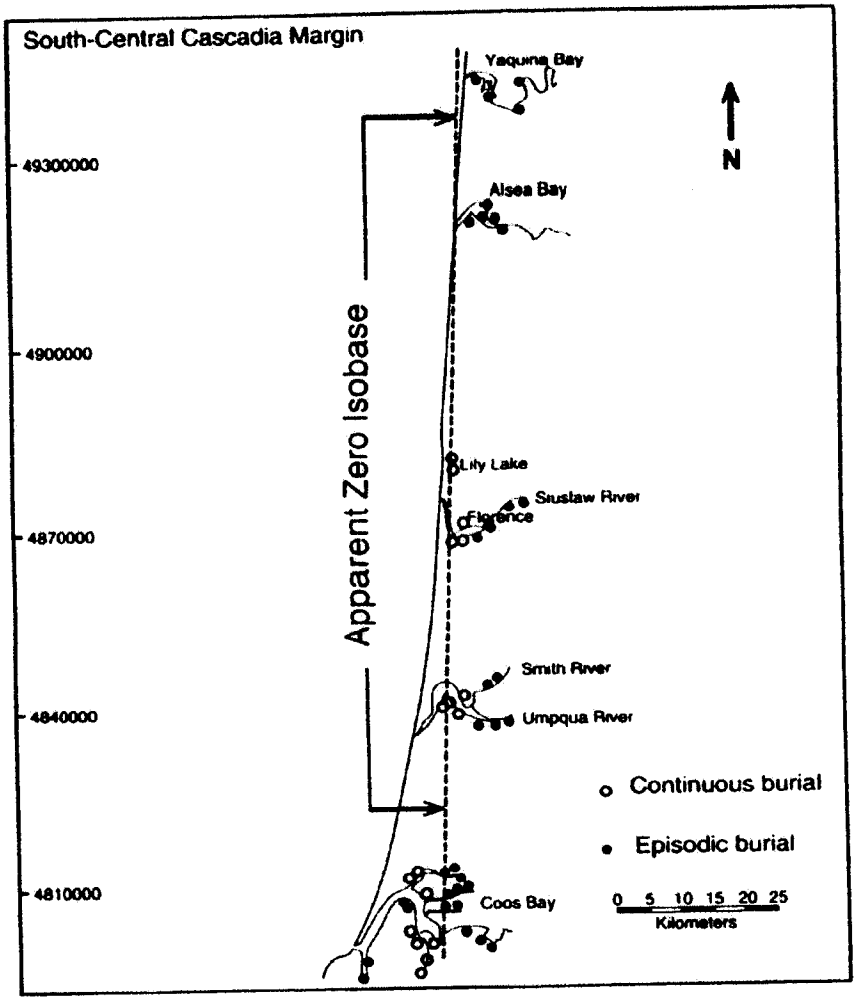

Figure 19. Pattern of paleosubsidence in south central Oregon from Briggs (1994 unpublished thesis). The open circles indicate areas with continuous peat development indicative of near zero paleosubsidence in an environment of rising sea level. Dots indic core sites with abrupt vertical changes in peat development characteristic of episodic paleosubsidence. The pattern of increasing subsidence inland is opposite that predicted the narrow ruptures of Scenario 1 (Models 1A-C) but approximates Scenario 2 (Models 2A-C). Compare to Figures 10-17 (see Figure 1 for geographic orientation).

The two segment ruptures (Models 2Cn and 2Cs, Figures 16 and 17) are basically the same a Scenario 2 but with half the vertical deformation. Paleoseismic data appears to favor the larg vertical deformation of the 1,050 km ruptures (Figures 20 and 21)

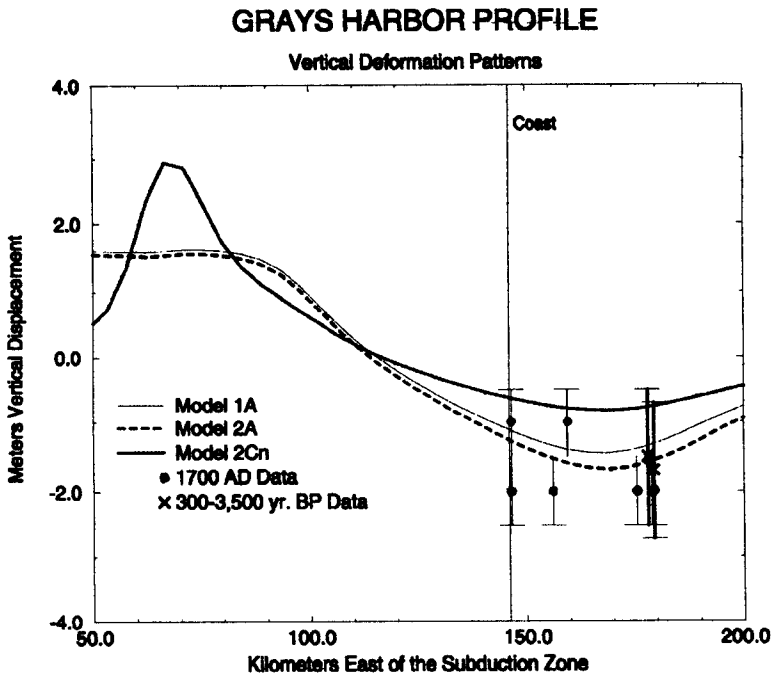

Figure 20. Cross section of vertical surface deformation showing the similarity of Models 1A and 2A at the latitude of Grays Harbor, Washington. Note the better fit of these models to the paleoseismic data relative to the segmentation model, Model 2Cn.

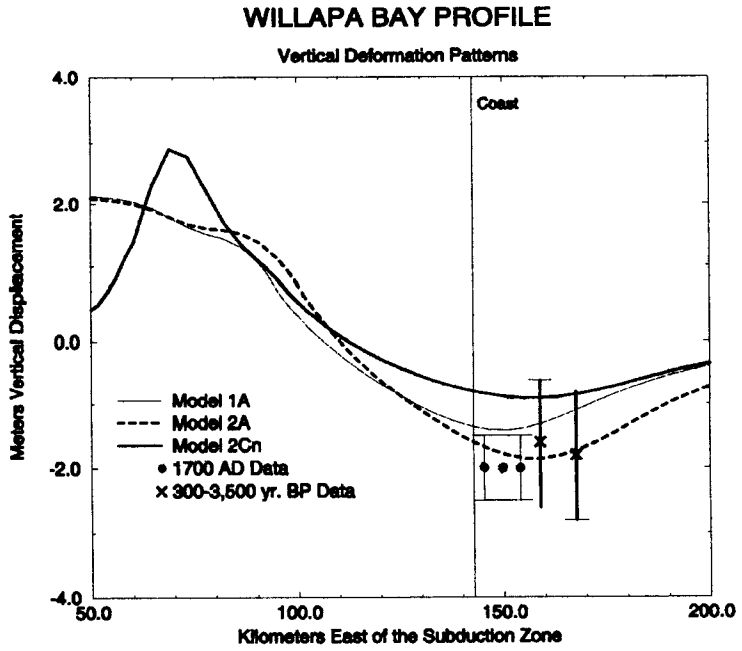

Figure 21. Cross section of vertical surface deformation showing the similarity of Models 1A and 2A at the latitude of Willapa Bay, Washington. Note the better fit of these models to the paleoseismic data relative to the segmentation model, Model 2Cn.

Figure 22 illustrates that, all other factors constant, variations of slip at the seaward transitio zone produce no differences in position or magnitude of subsidence at distances greater than km from the deformation front. Hence, as previously inferred (Figures 7-9), the onshore paleoseismic and geodetic data in the Cascadia subduction zone offer no constraints on the offshore deformation in the accretionary wedge.

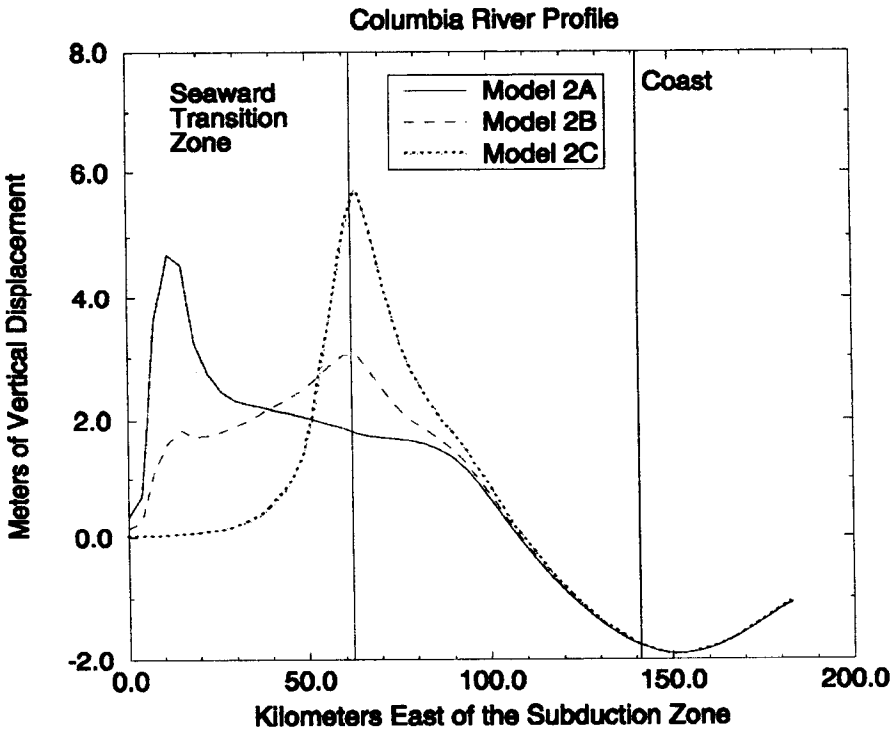

Figure 22. Cross section of vertical surface deformation from models with variable sli distribution in the seaward transition zone (STZ) but all other parameters held const Note how the onshore deformation that might be inferred from geodetic or paleoseism data offers no constraints on potential deformation in the STZ. Cross section trends west at the latitude of the Columbia River.

Figure 23 illustrates the quantitative estimates of paleoseismic subsidence in Oregon relativ the deformation profiles of Model 1A and 2A. Only the Columbia River estuary has enoug west width of paleoseismic data to show the overall variation. The match of Model 2A is somewhat better than 1A there (Figure 23a). Scatter in the quantitative paleoseismic data i large in the other profiles to provide much information, although there is some evidence of increasing subsidence inland at Netarts-Tillamook (Figure 23b), Yaquina Bay (Figure 23d), Siuslaw River (Figure 23f), and in the more qualitative reconnaissance soil coring in south Oregon (Figure 19). Inland decrease of estuarine water salinity may make the paleo-deform data less reliable, since much of the data relies on the sensitivity of estuarine flora to tidal s water (e.g. see Peterson and Darienzo, 1996; Peterson and others, 1997, for discussion).

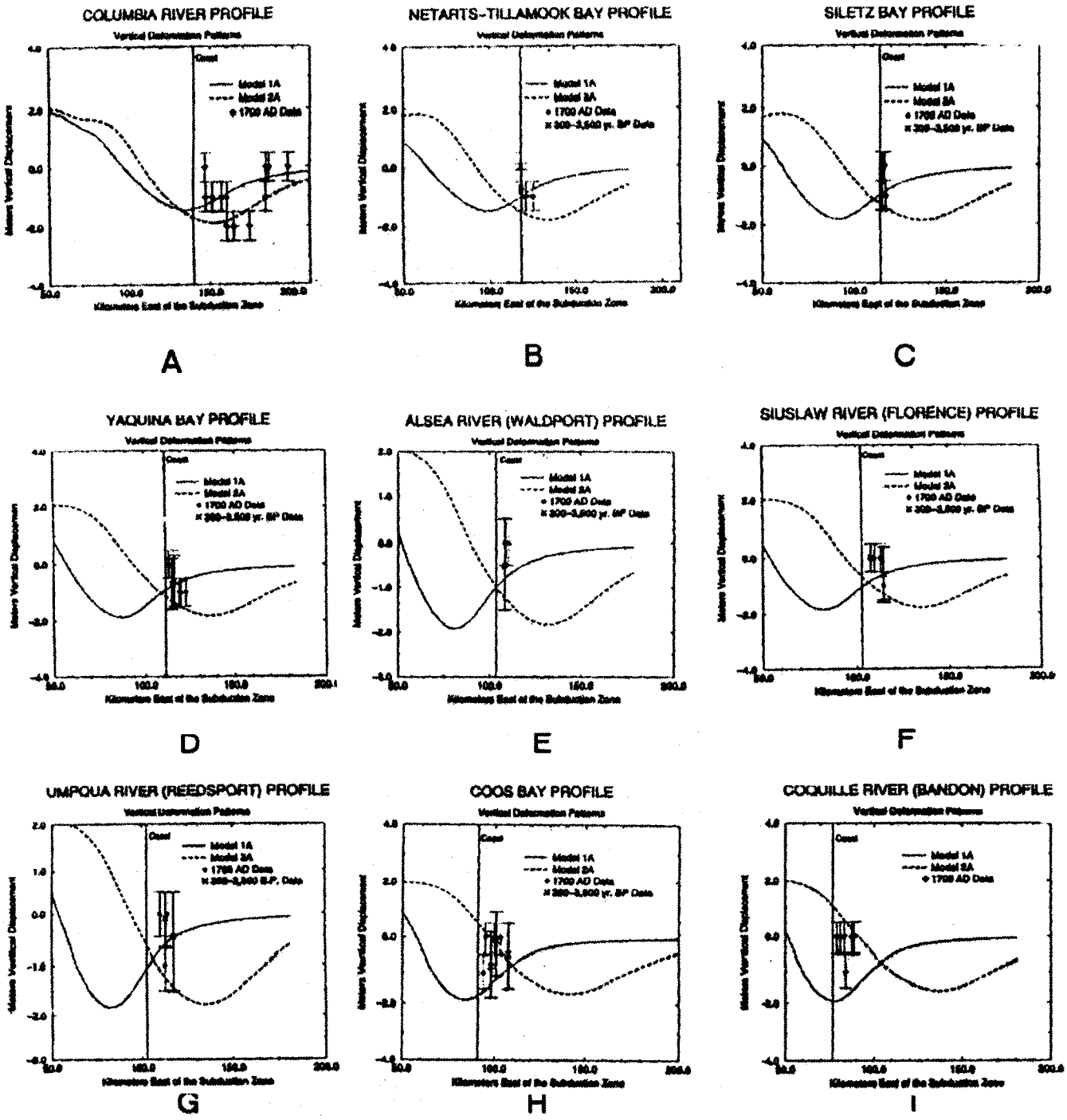

Figure 23A through 23I. Cross sections of vertical surface deformation showing the lateral offset of Scenarios 1 and 2, illustrated by Models 1A and 2A, at the latitude of Oregon estuaries with significant paleoseismic data. Note the better fit of wider rupture of Model 2A to the quantitative paleoseismic data at the Columbia River. Paleoseismic data to the south is from estuaries with limited east-west extent, so deformation trends are hard to interpret relative to data error. See Figure 1 for locations.

Tsunami Run-up

As illustrated by theoretical work of Tadepalli and Synolakis (1994), by producing a leading depression wave, an offshore trough of coseismic subsidence causes higher tsunami run-up than an onshore trough. Scenario lshould thus generate higher run-up than Scenario 2 in Oregon and northernmost California, other factors being equal. Figure 24 (Model 1A versus 2A), taken from data of Myers and others (1999), illustrates that the narrower rupture (1A) generated 40-50 percent higher run-up in Oregon and northern California. As expected, the segment ruptures with half of the slip of the 1,050 km ruptures produced about half the run-up elevation at the coast (Models 2Cs and 2Cn versus 2C, Figure 24).

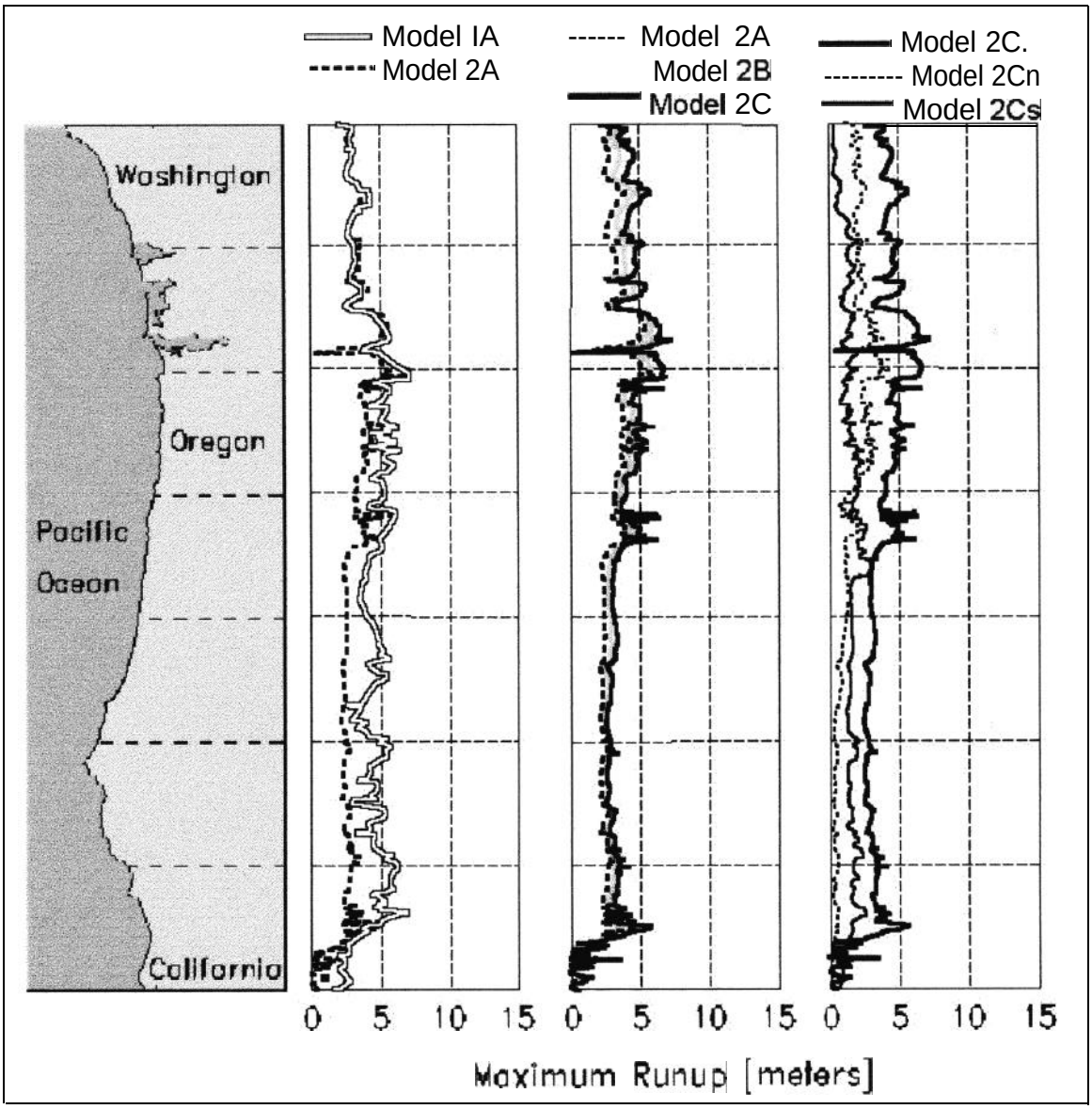

Figure 24. Maximum tsunami run-up elevation at the coast (Figure modified from Myers and others, 1999).

The intention of Scenarios A to C was to illustrate the effect of decreasing slip (and uplift) in the STZ. The anomalous spikes of uplift generated at the up dip tip of the buried ruptures compensated for the decreased slip across the STZ, so all of these scenarios had similar uplift for a given total slip (Figure 22). Run-up was therefore similar for all three, all other factors constant (e.g. Models 2A-C, Figure 24). Scenario C produced slightly higher run-up because the spike of uplift was closest to shore. Decreasing slip on a single buried rupture is probably not a realistic way to simulate decreasing slip in the STZ. A series of splay faults with progressively decreasing slip but rupturing to the surface would have been more realistic; however, even in this case total slip would necessarily be partitioned into a series of upward curving thrust faults with higher geometric uplift than the low dipping megathrust (Figure 2), so it is not clear whether the overall vertical deformation would be significantly different.

DISCUSSION

The eight rupture scenarios do a reasonable of job exploring variation in regional coseisrnic flexure of the North American plate resulting from uncertainties in slip, width, and length of ruptures, Explored are variations in rupture length of 1050-450 km, width from 70 km to 140 km in Oregon and northern California, and slip from 15-20 m to 9 m. An effective range of 50 to 0 percent aseismic slip (coupling ratio 0.5 to 1.0) is covered by these slip scenarios. Resulting tsunami run-up varied linearly with total fault slip, and narrow ruptures produced higher tsunami run-up than wide ruptures, all other factors equal.

Paleoseismic data appear to be most consistent with simulations that have 15-20 m of slip and wide (140 km or larger in Oregon and northern California), long (1050 km) ruptures. Correlation of simulations to paleoseismic data does not prove that large ruptures occur. Paleoseismic subsidence may not be coseismic with the main megathrust event, perhaps occurring hours or days afterward as result of aftershocks or viscoelastic adjustments (see discussion of viscoelastic models by Wang and others, 1994; Wang, 1995).

All of the simulations have some error from anomalous "spikes" of uplift at the seaward ends of the ruptures, and none of them consider partitioning of the slip into asperities, splay thrust faults, or clockwise rotating blocks within the North American Plate. Simulation of possible decrease in slip landward of the locked zone appears reasonable, but similar simulation of decreasing slip seaward of the locked zone in the accretionary wedge produced anomalous spikes of uplift. The net effect of these spikes was to produce similar vertical uplift and tsunami run-up regardless of slip distribution in the accretionary wedge. The total slip in all scenarios is probably about 13 percent too high in southernmost Washington, Oregon., and northern California, since partitioning of oblique convergence into clockwise rotating blocks of the North American Plate is not considered.

The 1964 Alaskan earthquake illustrates the importance of asperities and splay faults. The coseismic surface deformation there is consistent with 20-30 m of slip in a few central areas of the locked zone, decreasing to 1-6 m in adjacent areas along strike (Holdahl and Sauber, 1994). Significant slip in the Alaskan event was partitioned into a local thrust fault, causing dip slip of up

to 8 m over a length as much as 142 km (Plafker, 1972). Since this fault dips 52°-85°, much of the slip was expressed as vertical displacement. Coastal areas landward of local structures and asperities like those in Alaska could possibly receive much larger tsunamis than other areas. Future research should focus on discriminating where these zones of anomalous uplift might lie on the Cascadia margin.

Submarine landslides and turbidity currents associated with a great earthquake can also generate tsunamis. Landslides on the order of tens of kilometers wide have been mapped on the continental slope (e.g. Goldfinger and others, 1992b). None of the scenarios address this type of bottom deformation. Landslide susceptibility analysis of the continental slope will be needed to evaluate the importance of this source.

CONCLUSIONS

The most important sources of error for tsunami generation are the amount of slip and width of the rupture. Uncertainty in the coupling ratio is one of the most important errors in estimation of slip. A variation from an effective coupling ratio of 1.0 to 0.5 is covered by the scenarios. Total slip in all of the scenarios is probably about 13 percent too high in north-south trending parts of the margin, because the models ignored oblique convergence taken up by lateral faults in the North American Plate. South of the Colunibia River geophysical data indicates that ruptures are narrower than in Washington., but there is much uncertainty in absolute width owing to poorer geophysical data. Ruptures with widths of 70 and 140 km were simulated in this segment, covering most of the uncertainty. The wider ruptures are more consistent with available paleoseismic data and produce 40-50 percent lower tsunami run-up than the narrower ruptures. Paleoseisrnic data is permissive of 15-20 m of total slip consistent with ruptures on the order of 1000 km in length. The large uncertainties in the paleoseismic data do not allow these findings to be more than permissive constraints on rupture width and slip. The scenarios cover all possibilities for rupture penetration through the seaward transition zone (no penetration to complete penetration); however, for constant slip, tsunami run-up was equal for all degrees of penetration, owing to anomalous "spikes" of simulated uplift at the up dip tip of each rupture.

Lessons learned from this exercise include: (1) the Okada (1985) algorithm produces anomalous "spikes" of uplift exceeding the predicted geometric uplift by nearly a factor of 2 at the up-dip tip of thrust fault ruptures; (2) sirnulated thrust fault ruptures should therefore be extended to (or very near) the surface to minimize this source of error; (3) because of the "spike" effect, variations in slip across an accretionary wedge (seaward transition zone) are best simulated by a series of individual ruptures of varying displacement, each reaching the surface, rather than by varying slip on a single model fault plane; (4) paleoseismic data from estuarine marshes and geodetic information can offer important constraints on slip, width, and length of megathrust ruptures but not on the pattern of offshore deformation; (5) likely presence of asperities and splay faults that partition significant slip is a very large source of error; the 1964 Alaskan earthquake is a case in point; and (6) total potential coseismic slip is speculative, owing to uncertainties in aseismic slip, amount of main shock versus after shock slip, and potential post-seismic viscoelastic adjustments affecting paleoseisrnic subsidence estimates. In addition to these issues, submarine landslides are an additional source of tsunami excitation not treated in this investigation.

Characterization of tsunami sources is best addressed by a inter-disciplinary approach that incorporates geological, geophysical, and numerical modeling expertise.

ACKNOWLEDGMENTS

Hiroo Kanamori of the California Institute of Technology, Thomas S. Yelin and Samuel H. Clarke of the U.S. Geological Survey, and Robert S. Crosson of the University of Washington gave generously of their time in discussions of possible fault slip and magnitude for subduction zone earthquakes. Chris Goldfinger of Oregon State University contributed the estimated width of the seaward transition zone (accretionary wedge) and provided valuable criticism of the paper. The project was supported by grants from the Oregon Department of Justice and the U.S. Geological Survey's National Earthquake Hazard Reduction Program award number 1434-HQ096-6R-02712.

REFERENCES

Ando, M., 1975, Source mechanisms and tectonic significance of historic earthquakes along the Nankai trough, Japan: Tectonophysics, v. 27, p. 119-140.

Atwater, B.F., 1992, Geologic evidence for great Holocene earthquakes along the outer coast of Washington State: Journal of Geophysical Research, v. 97, p. 1901-1919.

Atwater, B. F., and Hemphill-Haley, E., 1996, Preliminary estimates of recurrence intervals for great earthquakes of the past 3500 year at northeastern Willapa Bay, Washington: U.S. Geological Survey Open-File Report 96-001, 87 p.

Atwater, B.F., Nelson, A.R., Clague, J.J., Carver, G.A., Yamaguchi, D.K., Bobrowsky, P.T., Bourgeois, J., Darienzo, M.E., Grant, W.C., Hemphill-Haley, E., Kelsey, H.M., Jacoby, G.C., Nishenko, S.P., Palmer, S.P., Peterson, C.D., and Reinhart, M.A., 1995, Summary of coastal geologic evidence for past great earthquakes at the Cascadia subduction zone: Earthquake Spectra, v. 11, no. 1, p. 1-18.

Briggs, G.G., 1994, Coastal crossing of the elastic strain zero-isobase, Cascadia margin, south central Oregon coast: Portland, Oregon, Portland State University masters thesis, Figure 19, p. 176,251 p.

Clague, J.J., 1997, Evidence for large earthquakes at the Cascadia subduction zone: Reviews of Geophysics, v. 35, no. 4, p. 439-460.

Darienzo, M.E., and Peterson, C.D., and Clough, C., 1994, Stratigraphic evidence for great subduction-zone earthquakes at four estuaries in northern Oregon, U.S.A.: Journal of Coastal Research, v. 10, no. 4, p. 850-876.

Darienzo, M.E.) and Peterson, C.D., 1995, Magnitude and frequency of subduction zone earthquakes along the northern Oregon coast in the past 3,000 years: Oregon Geology, v. 57, no. 1, p. 3-12.

Davis, E.E., and Hyndman, R.D., 1989, Accretion and recent deformation of sediments along the northern Cascadia subduction zone: Geological Society of America Bulletin, v. 101, p. 1465-1480.

DeMets, C., Gordon, RG., Argus, D.F., and Stein, S., 1990, Current plate motions: Geophysical Journal International, v. 10 1, p. 425-478.

Fleuck, P., 1996, 3-D dislocation model for great earthquakes of the Cascadia subduction zone: Zurich, Switzerland, Swiss Federal Institute of Technology Diploma Thesis, completed at University of Victoria, Victoria, B.C., Canada, 105 p.

Fleuck, P., Hyndman, R.D., and Wang, K., 1997, Three-dimensional dislocation model for great earthquakes of the Cascadia subduction zone, Journal of Geophysical Research, v. 102, no. 9, p. 20539-20550.

Geomatrix Consultants, 1995, 2.0, Seismic source characterization., *in* Geomatrix Consultants, Seismic design mapping, State of Oregon: Final Report prepared for Oregon Department of Transportation, Project No. 2442, p. 2-1 to 2-153.

Goldfinger, C., 1994, Active deformation of the Cascadia forearc: implications for great earthquake potential in Oregon and Washington: Corvallis, Oreg., Oregon State University Ph.D. thesis, 202 p.

Goldfinger, C., Kulm, L. D., Yeats, R.S., Applegate, B., MacKay, M.E., and Moore, G.F., 1992a, Transverse structural trends along the Oregon convergent margin: Geology, v. 20, p. 141-144.

Goldfinger, C., Kulm, L. D., Yeats, R.S., Mitchell, C., Weldon, R.E., III, Peterson, C.D., Darienzo, M.E., Grant, W., and Priest, G., 1992b, Neotectonic map of the Oregon continental margin and adjacent abyssal plain: Oregon Department of Geology and Mineral Industries Open-File Report O-92-4, 17 p.

Goldfinger, C., Kulm, L. D., Yeats, R.S., 1993, Oblique convergence and active strike-slip faults of the Cascadia subduction zone: Oregon margin [abstract]: EOS, Transactions of the American Geophysical Union, v. 74, no. 43, p. 200.

Goldfinger, C., Kulm, L. D., Yeats, R.S., 1994, An estimate of maximum earthquake magnitude on the Cascadia subduction zone: Geological Society of America Abstracts with Programs, v. 26, no. 7, p. A-525.

Goldfinger, C., McNeill, L.C., Kulm, L. D., and Yeats, R.S., 1996, Width of the seismogenic plate boundary in Cascadia: structural indicators of strong and weak coupling [abs.]: Geological Society of America Abstracts with Programs, v. 28, no. 5, p. 69.

Hebenstreit, G.T. and Murty, T.S., 1989, Tsunami Amplitudes from Local Earthquakes in the Pacific Northwest Region of North America Part 1: The Outer Coast, *Marine Geodesy*, 13(2), 101-146.

Holdahl, S.R., and Sauber, J., 1994, Coseismic slip in the 1964 Prince William Sound Earthquake: a new geodetic inversion: PAGEOPH, v. 142, no. 1, p. 55-82.

Huang, J., and Turcotte, D.L., 1990, Evidence for chaotic fault interactions in the seismicity of the San Andreas Fault and Nankai Trough: Nature, v. 348, p. 234-236.

Hyndman, R.D., and Wang, K., 1993, Thermal constraints on the zone of a major thrust earthquake failure: the Cascadia subduction zone: Journal of Geophysical research, v. 98, no. b2, p. 2039-2060.

Hyndman, R.D., and Wang, K., 1995, The rupture zone of Cascadia great earthquakes from current deformation and the thermal regime: Journal of Geophysical Research, v. 100, no. B11, p. 22,133-22,154.

Hyndman, R.D., Yorath, C.J., Clowes, R.M., and Davis, E.E., 1990, The northern Cascadia subduction zone at Vancouver Island: Seismic structure and tectonic history: Canadian Journal of Earth Science, v. 27, p. 313-329.

Kanamori, H., 1977, Seismic and aseismic slip along subduction zones and their tectonic implications, *in* Talwani, M,., and Pittman, W.C., eds., Island arcs, deep sea trenches and back-arc basins: Maurice Ewing series, American Geophysical Union, v. 1, p. 163-174.

McCaffrey, R., and Goldfinger, C., 1995, Forearc deformation and great subduction earthquakes: implications for Cascadia offshore earthquake potential: Science v. 267, p. 856-859.

Myers, E., Baptista, A.M., and Priest, G.R., 1999, Finite element modeling of potential Cascadia subduction zone tsunamis: Science of Tsunami Hazards, v. 17, p. 3-18.

Nelson, A. R., Atwater, B. F., Bobrowsky, P. T., Bradley, L., Clague, J. J., Carver, G. A., Darienzo, M. E., Grant, W. C., Krueger, H. W., Sparkes, R., Stafford, T. W., Jr., and Stuiver, M., 1995, Radiocarbon evidence for extensive plate-boundary rupture about 300 years ago at the Cascadia subduction zone: Nature, v. 378, no. 23, p. 371-374.

Okada, Y., 1985, Surface deformation due to shear and tensile faults in a half-space: Bulletin of the Seismological Society of America, v. 75, no. 4, p. 1135-1154.

Peterson, C. D., Barnett, E.T., Briggs, G.G., Carver, G.A., Clague, J.J., and Darienzo, M.E., 1997, Estimates of coastal subsidence from great earthquakes in the Cascadia subduction zone, Vancouver, Island, B.C., Washington, Oregon, and northernmost California: Oregon Department of Geology and Mineral Industries Open-File Report O-97-5, 44 p.

Peterson, C.D., and Darienzo, M.E., 1996, Discrimination of climatic, oceanic, and tectonic mechanisms of cyclic marsh burial, Alsea Bay, Oregon, *in* Rogers, A.M., Kockleman, W.J., Priest, G.R., and Walsh, T.J. eds., Assessing and reducing earthquake hazards in the Pacific Northwest: U.S. Geological Survey Professional Paper 1560, p. 115-146.Peterson, C.D., and Priest, G.R., 1995, Preliminary reconnaissance of Cascadia paleotsunami deposits in Yaquina Bay, Oregon: Oregon Geology, v. 57, p. 33-40.

Peterson, C.D, and Priest, G.R., 1995, Preliminary reconnaissance survey of Cascadia paleotsunami deposits in Yaquina Bay, Oregon: Oregon Geology, v. 57, no. 2, p. 33-40.

Plafker, G., 1972, Alaskan earthquake of 1964 and Chilean Earthquake of 1960: implications for arc tectonics: Journal of Geophysical Research, v. 77, p. 901-925.

Priest, G. R., 1995, Explanation of mapping methods and use of the tsunami hazard maps of the Oregon coast: Oregon Department of Geology and Mineral Industries Open-File Report O-95-67, 95 p.

Riddihough, R.P., 1984, Recent movements of the Juan de Fuca plate system: Journal of Geophysical Research, v. 89, p. 6980-6994.

Rogers, G.C., 1988, An assessment of the megathrust earthquake potential of the Cascadia subduction zone: Canadian Journal of Earth Science, v. 25, p. 844-852.

Satake, K., Shemazaki, K., Yoshinobu, T., and Ueda, K., 1996, Time and size of a giant earthquake in Cascadia inferred from Japanese tsunami records of January 1700: Nature, v. 379, no. 6562, p. 246-249,

Savage, J.C., 1983, A dislocation model of strain accumulation and release at a subduction zone: Journal of Geophysical Research, v. 88, p. 4984-4996.

Scholz, C. H., 1982, Scaling laws for large earthquakes: consequences for physical models: Bulletin of the Seismological Society of America, v. 72, no. 1, p. l-14.

Tadepalli, S., and Synolakis, C.E., 1994, The run-up of N-waves on sloping beaches: Proceedings of the Royale Society of London, v. A445, p. 99-112.

Wang, K., 1995, Coupling oftectonic loading and earthquake fault slips at subduction zones: PAGEOPH, v. 145, nos. 3 and 4, p. 537-559.

Wang, K., Dragert, H., and Melosh, H.J., 1994, Finite element study of uplift and strain across Vancouver Island: Canadian Journal of Earth Science, v. 31, p. 1510-1522.

Whitmore, P. M., 1993, Expected tsunami amplitudes and currents along the North American coast for Cascadia subduction zone earthquakes: Natural Hazards, v. 8, p. 59-73.

Whitmore, P. M., 1994, Expected tsunami amplitudes off the Tillamook County, Oregon, coast following a major Cascadia subduction zone earthquake: Oregon Geology, v. 56, no. 3, p. 62-64.

COMPARING MODEL SIMULATIONS OF THREE BENCHMARK TSUNAMI GENERATION CASES

Philip Watts
Applied Fluids Engineering, PMB #237, 5710 E. 7th Street, Long Beach, CA 90803
Fumihiko Imamura
Professor, Disaster Control Research Center, School of Engineering, Tohoku University, Aoba 06, Sendai 980-8579, Japan.
Stéphan Grilli
Professor, Department of Ocean Engineering, University of Rhode Island, Narragansett, RI 02882

ABSTRACT

Three benchmark cases are proposed to study tsunamis generated by underwater landslides. Two distinct numerical models are applied to each benchmark case. Each model involves distinct center of mass motions and rates of landslide deformation. Computed tsunami amplitudes agree reasonably well for both models, although there are differences that remain to be explained. One of the benchmark cases is compared to laboratory experiments. The agreement is quite good with the models. Other researchers are encouraged to employ these benchmark cases, in future experimental or numerical work.

performed laboratory experiments. Each case is two-dimensional in order to reduce computational or experimental effort.

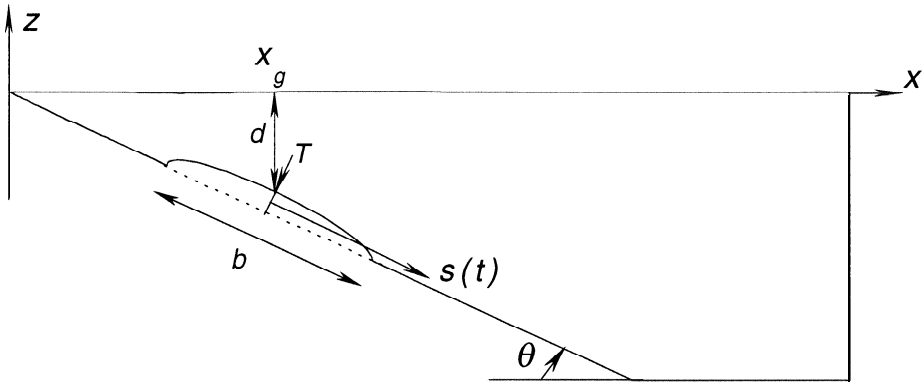

Figure 1: Definition sketch of the simulation domain in II and GW Models, and of initial landslide parameters

We compare results from two distinct numerical models. We hope that this work will promote future numerical andexperimental comparisons. The comparisons made here are by no means the end of this effort.

BENCHMARK CASES

To facilitate their experimental realization, the benchmark cases chosen for this work are based in part on the sliding block experiments of previous researchers (Heinrich, 1992; Iwasaki, 1982; Watts, 1997; Wiegel, 1955). A straight incline forms a planar beach with the coordinateorigin at the undisturbed beach and the positive x-axis oriented horizontally away from the shoreline (Fig. 1). A semi-ellipse approximates the initial landslide geometry. Landslide deformation is permitted following incipient motion of the semi-ellipse. The nominalunderwater landslidelength measured along the incline is b =lOOO m for all three cases. All underwater landslides are assumed to havea bulk density ρ_b =1900 kg/m^3 and fail in sea water of density ρ_o =1030 kg/m^3. The geometrical parameters for each benchmark case are given in Table 1. The initial submergence at the middle of the landslide, $x = x_g$, was obtained from a scaled reference equation $d = b \sin\theta$, while the initiallandslide thickness was calculatedfrom another scaled reference equation, 7' = 0.2 b $\sin\theta$ (Watts et al., 2000). A wave gage was situated above the middle of the initial landslide position at $x_g = (d + T/\cos\theta)/\tan\theta$, and recorded tsunami elevation $\eta(t)$.

Dimensional quantities are presented throughout since different numerical techniques employ different non-dimensional schemes. Watts (1998) provides the correct Froude scaling to perform these benchmark experiments at laboratory scale.

Table 1: Underwater landslide and numerical wave gage parameters for benchmark cases c_1, c_2, and c_3

Case	θ	b (m)	T (m)	d (m)	x_g (m)
(1)	(2)	(3)	(4)	(5)	(6)
c_1	30°	1000	100	500	1066
c_2	15°	1000	51.8	259	1166
c_3	5°	1000	17.4	87.2	1196

LABORATORY EXPERIMENTS

Laboratory experiments were conducted in the University of Rhode Island wavetank (length 30 m, width 3.6 m, depth 1.8 m). This tank is equipped with a modular beach made of 8 independently adjustable panels (3.6 m by 2.4 m) whose difference in slope can be up to 15°. Benchmark case 2 was tested in the wave tank at 1: 1000 scale, in the set-up shown in Fig. 2. Two beach panels were set to an angle $\theta = 15°$ and covered by a smooth aluminium plate. A quasi two-dimensional experiment was realized by building vertical (plywood) side walls at a small distance (about 15 cm) from each other. A semi-elliptical wood and plastic landslide model was built and installed in between the walls. The model was equipped with low-friction wheels and a lead ballast was added to achieve the correct bulk density (Fig. 3). An accelerometer was attached to the model center of gravity to measure landslide kinematics. Four capacitance wave gages were mounted on an overhead carriage, to measure free surface elevation (Fig. 2), the first gage being located at $x = x_g$ and the others mounted 30 cm apart with increasing x-positions. Experiments were repeated at least five times and the repeatability of results was very good. Results are presented in a following section.

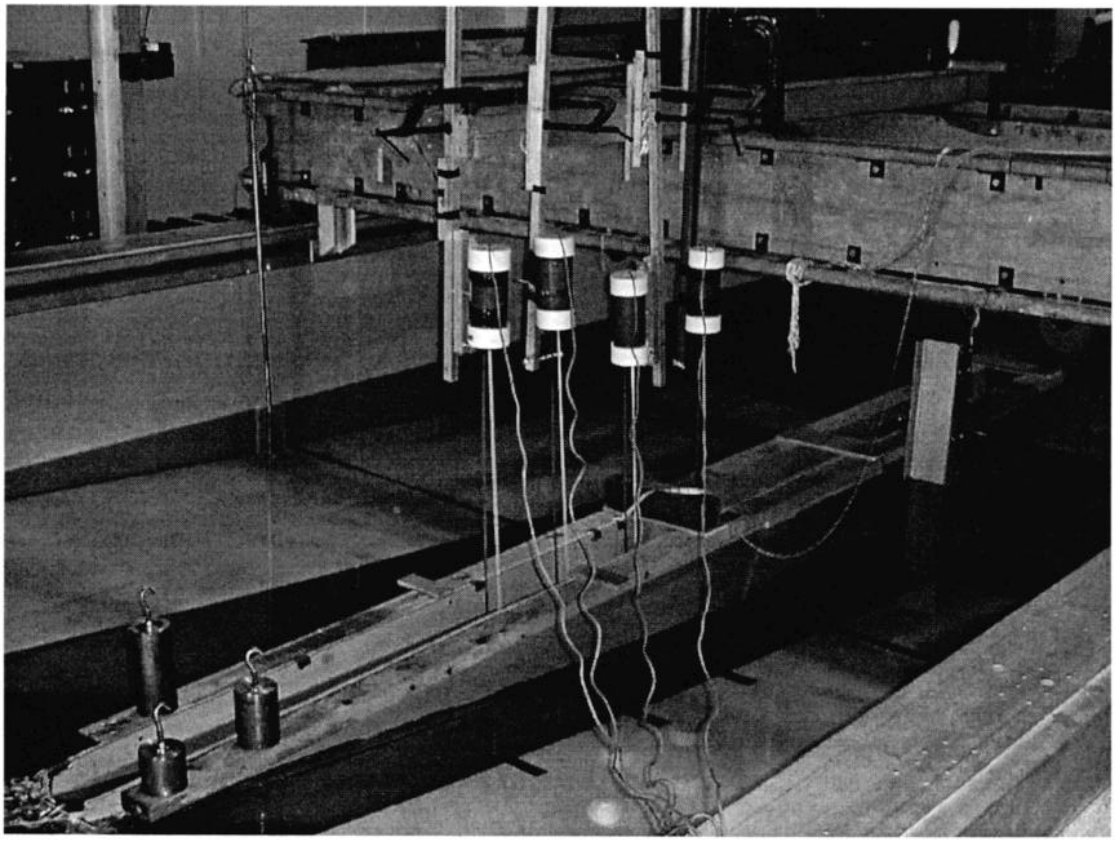

Figure 2: Quasi two-dimensional landslide experiments for benchmark case 2

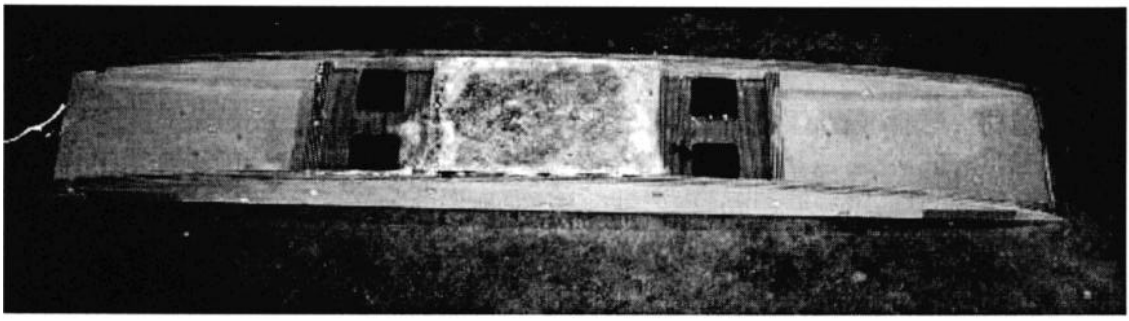

Figure 3: Close-up of scale model for two-dimensional landslide experiments

NUMERICAL MODEL DESCRIPTIONS

Imamura and Imteaz (1995) developed a mathematical model for a two-layer flow along a non-horizontal bottom. Conservation of mass and momentum equations were depth-integrated in each layer, and nonlinear kinematic and dynamic conditions were specified at the free surface and at the interface between fluids. Both fluids had uniform densities and were immiscible. Vertical velocity distributions were assumed within each fluid layer. The landslide fluid was ascribed a uniform viscosity, which sensitivity analyses show has very little effect on wave records over a range of viscosities 1-100 times that of water. A staggered leap-frog finite difference scheme, with a second-order truncation error was used to solve the governing equations. Landslides were thus modeled as immiscible fluid flows comprising a second layer, as in the work of Jiang and LeBlond (1992, 1993, 1994). An instantaneous local force balance governed landslide motion. Hence, this motion resulted from the solution of the problem itself and was not externally specified as a boundary condition. We will refer to this numerical model as the II Model below.

Grilli *et al.* (1989, 1996) developed and validated a two-dimensional Boundary Element Model (BEM) of inviscid, irrotational free surface flows (i.e., potential flow theory). Cubic boundary elements were used for the discretization of boundary geometry, combined with fully nonlinear boundary conditions and second-order accurate time updating of free surface position. The model was experimentally validated for long wave propagation and runup or breaking over slopes by Grilli *et al.* (1994, 1998). Model predictions are surprisingly accurate; for instance, the maximum discrepancy for solitary waves shoaling over slopes is 2% at the breaking point, between computed and measured wave shapes. Grilli and Watts (1999) applied this BEM model to water wave generation by underwater landslides and performed a sensitivity analysis for one underwater landslide scenario. The landslide center of mass motion along the incline was prescribed by the analytical solutions of Watts (1998, 2000) (see next section). In these computations, the landslide retained its semi-elliptic shape while translating along the incline. We will refer to this numerical model as the GW Model below.

Both the II and GW Models are used in the following to simulate tsunamis generated by underwater landslides of identical initial characteristics corresponding to the three benchmark cases in Table 1. For discretization techniques and numerical parameters used in both models, please refer to Imamura and Imteaz (1995) and Grilli and Watts (1999).

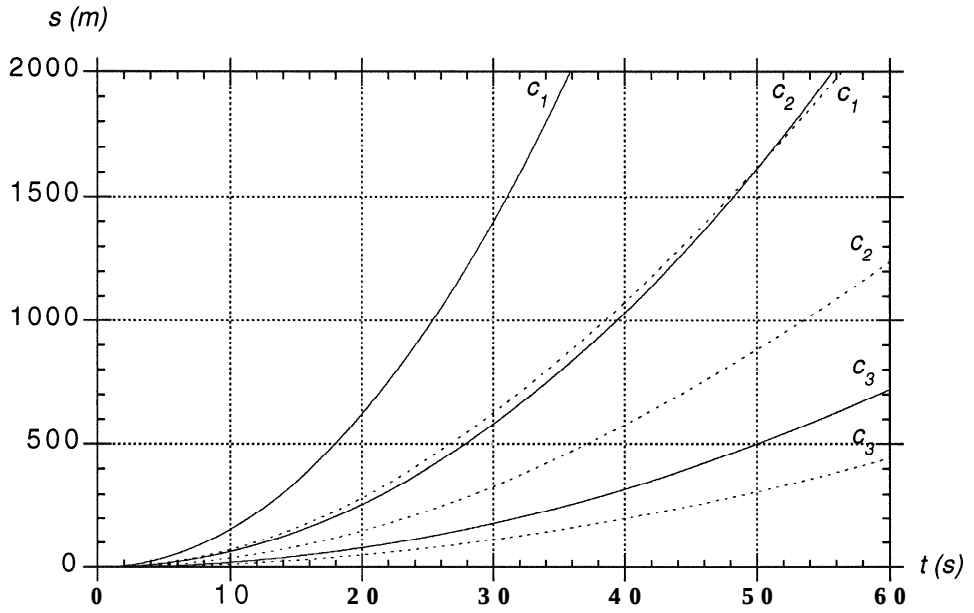

Figure 4: Underwater landslide center of mass motion as a function of time in the II (solid) and GW (dashed) Models, for benchmark cases c_1, c_2, and c_3 in Table 2

SIMULATION RESULTS

Descriptions of tsunami generation by underwater landslides should begin by documenting landslide center of mass motion and rates of deformation. Since both motion and deformation were prescribed in the GW Model, we proceed to describe the results obtained from the II Model and compare these results with the GW Model. We also relate the measured initial acceleration obtained for case 2. Assuming the center of mass motion $s(t)$ is parallel to the incline (Fig. 1), Fig. 4 shows the center of mass motions obtained in the II Model for the three benchmark cases. It is readily verified that the simple equation

$$s(t) = \frac{a_0 t^2}{2} \tag{1}$$

provides an accurate fit of these motions. Eq. (1) is the first term in a Taylor series expansion of landslide motion beginning at rest (Watts, 2000). In fact, two-parameter curve fits of the equation of motion given in Watts (1998) (and reproduced as Eq. (3) below) failed to produce unique parameter values, due to the accuracy of the one-parameter fit given by Eq. (1). Two curve fitting parameters introduced a redundancy in the solution algorithm that yielded infinite fitted solutions. Values of initial landslide accelerations a,

for the II Model obtained by curve fitting Eq. (1) can be found in Table 2. Note that R^2 coefficients were 0.99 or better for all of the fits. The experimental initial acceleration was a, = 0.73 m/s^2 for case 2. This compares favorably with the value from the GW Model in Table 2 and suggests an added mass coefficient $C_m \approx$ 1.2 given negligible rolling friction (see Eq. 5 below).

Table 2: Initial accelerations, terminal velocity and rates of deformation in II and GW Models

Case (1)	a_{oII} (m/s^2) (2)	a_{oGW} (m/s^2) (3)	u_{tGW} (m/s) (4)	Γ_{II} (s^{-1}) (5)	Γ_{GW} (s^{-1}) (6)
c_1	3.11	1.47	80.9	0.062	0.000
c_2	1.29	0.76	57.8	0.035	0.000
c_3	0.40	0.26	33.2	0.017	0.000

Landslide deformation in the II Model was manifested foremost as an extension in time, $b(t)$, of the initial landslide length b_o. Fig. 5 demonstrates that the non-dimensional ratio b/b_o varies almost linearly with time, following an initial transient, similar to the experimental observations made by Watts (1997) for a submerged granular mass. A semi-empirical expression that describes landslide extension is

$$b(t) = b_o \{1 + \Gamma t [1 - \exp(-Kt)]\} \quad (2)$$

where Γ is the eventual linear rate of extension and the exponential term describes an initial transient, with $K = a_o/g\Gamma$ (Watts *et al.*, 2000). The parameter K is chosen to fix the uppermost landslide corner in place as the center of mass begins to accelerate. Table 2 gives values of Γ for the II Model found from curve fits of Eq. (2).

Watts (1998) developed a wavemaker formalism for non-deforming underwater landslides, based on an analytical solution of center of mass motion

$$s(t) = s_o \ln \left[\cosh \left(\frac{t}{t_o}\right)\right] \quad (3)$$

with

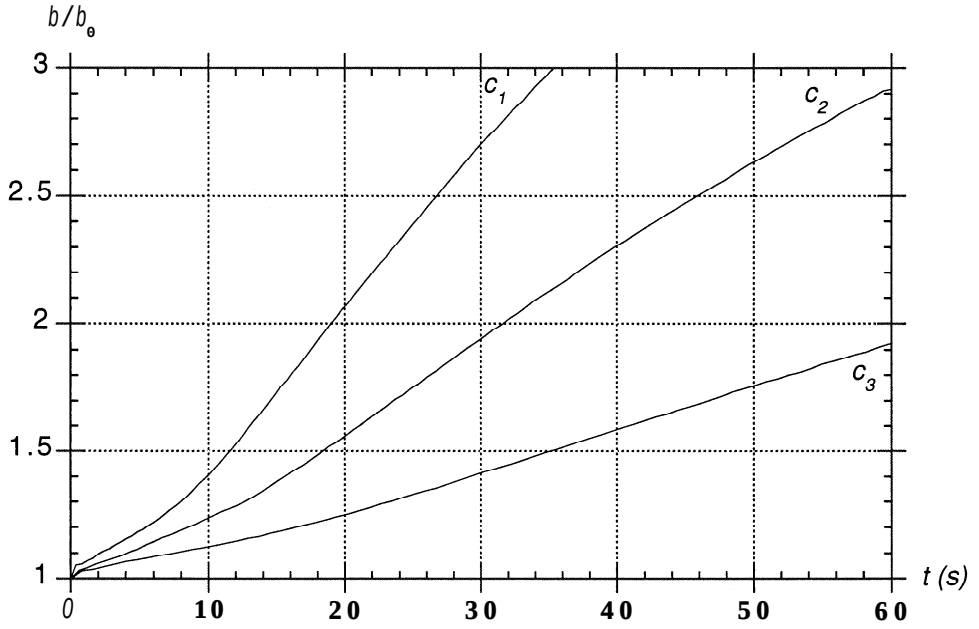

Figure 5: Underwater landslide temporal extension in II Model

$$s_o = \frac{u_t^2}{a_o} \quad , \quad t_o = \frac{u_t}{a_o} \tag{4a,b}$$

where a, and u_t denote landslide initial acceleration and terminal velocity, respectively (see Eq. (5) and discussion in the following section). Eqs. (3) and (4) were used in the GW Model to specify the landslide kinematics. Eq. (4) can also be expressed as a function of the landslide physical parameters initial length, incline angle, and density (Watts, 1998). For the three benchmark cases, using the data in Table 1, we find the values of a, and u_t listed in Table 2 and corresponding motion $s(t)$ shown in Fig. 4. Note, as discussed above, no extension Γ was specifiedin the GW Model.

Figures 6-8 show the tsunami simulation results of both numerical models for cases l-3, respectively. The GW and II Model results agree qualitatively for all three cases, although the GW Model produces slightly smaller wave amplitudes. The II Model produces more acute free surface curvature near $t = 0$ as well as longer tsunami periods. Maximum tsunami amplitudes at the numerical wave gages are given in Table 3. This is the same characteristic tsunami amplitude employed in the scaling analyses of Watts (1998, 2000). Note, the II Model has water wave disturbances in the first 5-20 s of each simulation brought on by a Kelvin-Helmholtz type instability along the landslide-water interface.

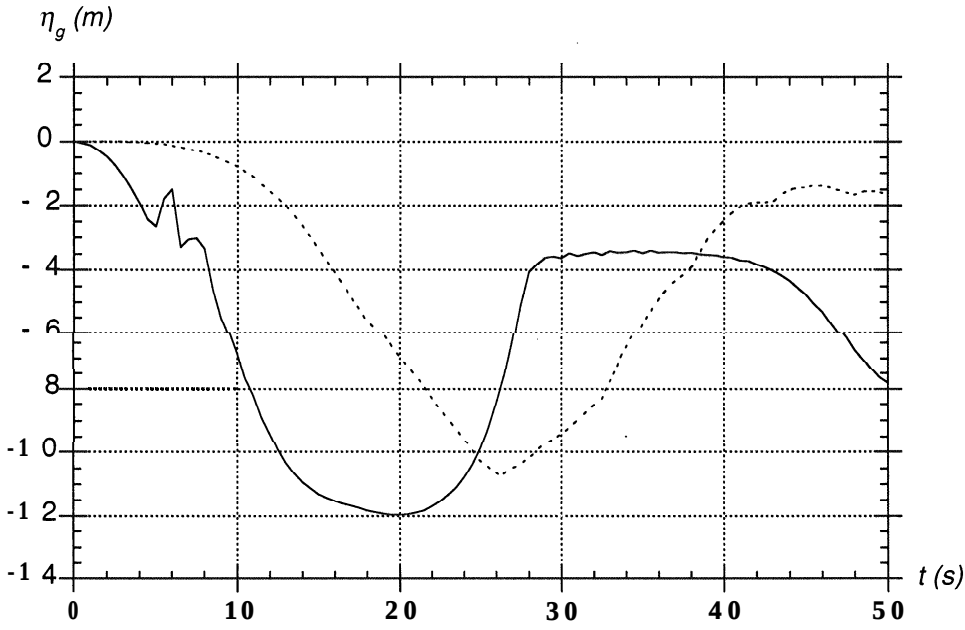

Figure 6: Numerical wave gage record at x_g = 1066 m for benchmark case 1; II Model (solid); GW Model (dashed)

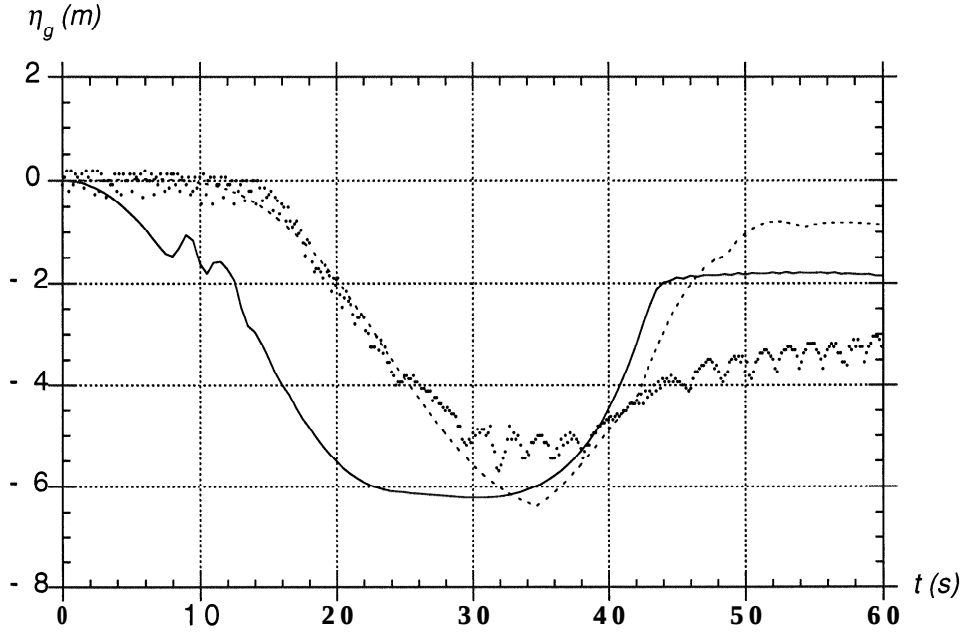

Figure 7: Numerical wave gage record at x_g = 1166 m for benchmark case 2; II Model (solid); GW Model (dashed); scaled-up experiments (dots)

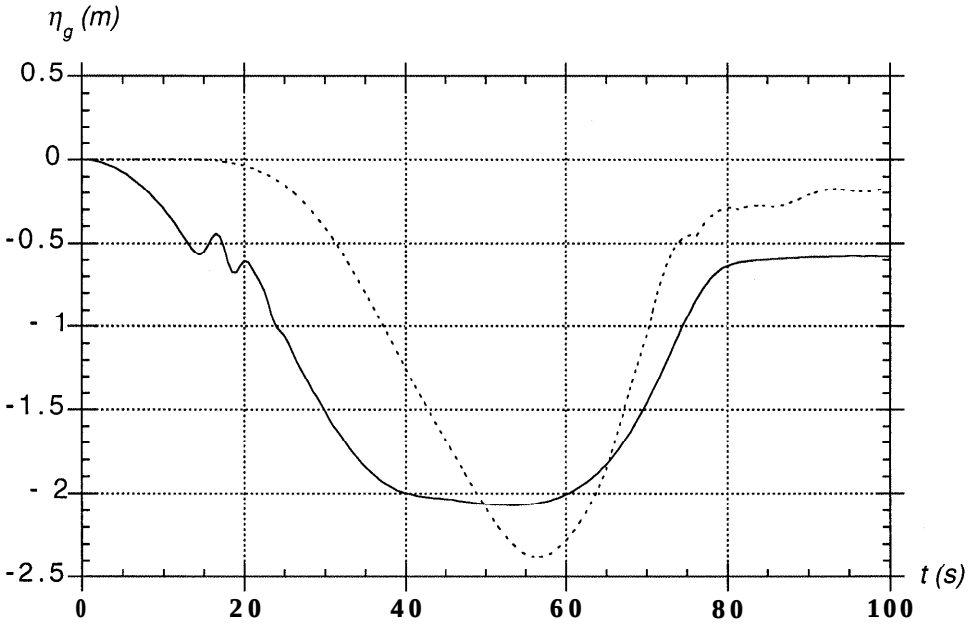

Figure 8: Numerical wave gage record at x_g = 1196 m for benchmark case 3; II Model (solid); GW Model (dashed)

Table 3: Simulated and calculated characteristic wave amplitudes

Case (1)	η_{II} (m) (2)	η_{GW} (m) (3)	η_{PP} (m) (4)
c_1	11.98	10.86	15.71
c_2	6.22	6.37	8.14
c_3	2.07	2.39	2.73

DISCUSSION

Tsunami generation in the shallow water wave limitoccurs through verticalacceleration of some region on the ocean floor (Tuck and Hwang, 1972; Watts *et al., 2000).* Since the center of mass motion modeled in the II Model, as shown in Fig. 4, corresponds to the landslide acceleration described by Eq. (1), tsunami generationby the II Model in Figs. 6-8 can be directly associated with vertical landslide acceleration. Tsunami generation in a potential flow model such as the GW Model, however, occurs through gradients of the

velocity potential at the free surface, which can arise from both horizontal and vertical landslide motions. Also, tsunami generation in the GW Model is theoretically not lirnited to landslide acceleration and may include the instantaneous water velocity distribution.

The initial center of mass motion during landslide tsunami generation can be accurately described by Eq. (1), assuming the correct initial acceleration is known. Along an infinite incline, an equation such as (3) provides a better description of the motion. Watts (1998) provides an analytical method for choosing between Eqs. (1) and (3) based on the length of the incline.

Tsunami amplitude is scaled by the landslide initial acceleration (Watts, 1998, 2000). The initial accelerations listed in Table 2 differ considerably between the two models, despite identical initial landslide shapes and bulk densities. The theoretical initial acceleration specified in the GW Model is, neglecting Coulomb friction,

$$\frac{a_o}{g} = \frac{(\gamma - 1)\sin\theta}{\gamma + C_m} \tag{5}$$

in which γ represents the landslide specific density and C_m an added mass coefficient. Eq. (5) applies specifically to underwater landslides that experience negligible basal friction due to phenomena such as water injection or liquefaction (Watts *et al.*, 2000). The value $C_m = 1$ used in the GW Model produces conservative landslide motions. Our experimental results suggest that $C_m = 1$ is a reasonable estimate of the actual added mass coefficient. If $C_m \approx 0$ were a better approximation for underwater landslide motion, then the GW Model initial accelerations listed in Table 2 would increase by about 50%, and would agree better with those of the II Model. A vanishing added mass coefficient may be more representative of the initial accelerations found from a depth-averaged model. Indeed, the initial acceleration found in the II Model for case 3 agrees well with Eq. (5), if $C_m \approx 0$. This is the least inclined slope studied. However, the initial accelerations found in the II Model for cases 1 and 2, which have larger incline angles, were larger than the corresponding maximal values from Eq. (5) with $C_m \approx 0$. This contradicts Eq. (5), which was derived for rigid body motion.

The additional center of mass acceleration in the II Model can be explained by landslide deformation. Landslide deformation shifts mass forward (during formation of a landslide nose) and results in an advance of the center of mass. The rapid shift in center of mass

experienced in the II Model may arise from model assumptions that are not present in actual underwater landslides. The rates of landslide extension reported in Table 2, for the II Model, are 3-6 times greater than the maximum rate

$$\Gamma_{\max} \approx \frac{\sqrt{\sin\theta}}{6}\sqrt{\frac{g}{b_o}} \tag{6}$$

estimated by Watts *et al.* (2000). These large rates of extension may arise from the assumption that the landslide behaves like an immiscible, homogeneous fluid with relatively low viscosity. A non-deforming landslide has infinite viscosity. For rates of extension given by Eq. (6), Watts *et al.* (2000) show that there is very modest change in the shape of the wave gage record. One such change is an increase of the curvature around $t = 0$, similar to the results from the II Model. The additional curvature shown in Figs. 6-8 can therefore be ascribed to landslide deformation.

We also note that the experimental work of Watts (1997) showed diminished wave amplitudes from deforming underwater landslides. This was an experimental artifact produced by flow through the granular media used to reproduce a landslide at laboratory scale. Watts *et al.* (2000), however, showed very small changes in characteristic wave amplitude with the GW Model when using rates of extension given by Eq. (6). Characteristic wave amplitudes were either increased or decreased depending on the incline angle. This suggests a complex relationship between landslide extension and tsunami amplitude.

A characteristic tsunami amplitude can form the basis of wavemaker curves and provide a valuable tsunami scaling quantity (Watts, 1998, 2000). The characteristic tsunami amplitude chosen here is the maximum depression measured by the wave gages in Figs. 6-8. Table 3 summarizes the characteristic tsunami amplitudes obtained for each benchmark case. Tsunami amplitudes from the two models differ by -10% to + 13%, as the incline angle decreases. These amplitudes compare favorably with the analytical prediction of Pelinovsky and Poplavsky (1996) for the same landslide parameters, denoted by PP in Table 3. While discrepancies remain, there is general agreement over the characteristic tsunami amplitudes.

Larger initial accelerations produce larger tsunami amplitudes. The change in characteristic amplitude can be quantified by choosing an effective landslide density. We calculate the

expected increase in wave amplitude for the II Model by calculating an effective specific density from Eq. (5) (with C_m = 1), using the observed center of mass acceleration produced by the II Model (Table 2). For case 2, for instance, the specific density γ = 3.07 reproduces an equivalent center of mass motion, using Eqs. (1) and (5), to that measured for the II Model. We now employ curve fits of characteristic amplitude versus specific density given by Watts *et al.* (2000) to scale the tsunami amplitude. We find a factor of 1.6 increase in wave amplitude for case 2 due to the increase in effective landslide density. This correction is made possible by a rigorous analysis of landslide motion. Hence, if the II Model had reproduced an initial acceleration equal to that of the GW Model for case 2, then we would expect the wave record shown in Fig. 7 to be 1.6 times smaller. Repeating this correction for all of the benchmark cases, we would find that wave records from the II Model would become smaller than wave records from the GW Model. Once the characteristic amplitude is corrected for the different initial accelerations, the remaining differences in characteristic amplitude between the two models are primarily due to depth averaging and landslide deformation. Hence, in view of these results, we conclude that depth averaging of the equations in the II Model leads to reduced tsunami amplitudes.

We repeat here model differences that could account for the results in Figs. 6-8. The GW Model solves a full set of fluid dynamic equations whereas the II Model depth-averages the flow in each fluid layer. The GW Model prescribes center of mass motion with Eqs. (3) to (5) and does not simulate landslide deformation. The II Model allows the landslide fluid to deform while undergoing motion derived from a local force balance. Qualitative differences in tsunami generation may be drawn from the comparisons made herein. Tsunami amplitudes, once corrected to match initial accelerations, may be larger in the GW Model due to the combined influences of both horizontal acceleration and landslide velocity on wave generation. If this is true, then the effective density of the II Model increases tsunami amplitude, while depth averaging decreases tsunami amplitude. The net effect leads to reasonable agreement between the two models. The general agreement in tsunami amplitude between the two models should probably be viewed as an outcome of some mean value theorem: the large number of mechanically plausible assumptions built into each model tends to produce similar outputs. More controlled comparisons of model results, however, are required in the future. Finally, a consequence of this work is that landslide tsunami generation, made with numerical models based on the seminal work of Jiang and Leblond (1992, 1993, 1994), i.e., using depth-averaged NSW equations, appears to have the potential to consistently under-predict tsunami amplitude, if rates of landslide deformation are not large.

CONCLUSIONS

Three benchmark cases for tsunamis generated by underwater landslides are proposed in this paper. These benchmark cases are considerably tsunamigenic and reinforce the significant hazard of tsunami generation by submarine mass failure in general. The underwater landslide initial acceleration and rate of deformation are both needed to compare benchmark simulations or experiments. Underwater landslide center of mass motion during tsunami generation can be described by the initial acceleration in Eqs. (1) and (5) whenever rates of landslide extension are less than values indicated by Eq. (4). Experimental results and numerical simulations to date indicate that the primary mode of landslide deformation consists of a linear rate of extension. Larger initial accelerations produce larger tsunami amplitudes. The characteristic tsunami amplitudes differed by up to 13% for the two numerical models compared here. Experimental results available for benchmark case 2 showed a better agreement with the GW Model results, in part because landslide deformation changes the shape of the wave gage record. Depth-averaged tsunami generation appears to underpredict tsunami amplitude. Further interpretation of existing model differences awaits more detailed model comparisons. We have endeavored to begin a process of comparing numerical simulations and experimental realizations for three benchmark cases. We hope the process will continue.

ACKNOWLEDGEMENTS

This work arose from a discussion at the 1999 IUGG General Meeting in Birmingham, U. K. at which time all tsunami scientists were invited to participate in landslide tsunami benchmark simulations. The authors are grateful for support from Applied Fluids Engineering, Inc. and the Disaster Control Research Center at Tohoku University.

REFERENCES

Assier Rzadkiewicz, S., Mariotti, C., and Heinrich, P. (1997). "Numerical simulation of submarine landslides and their hydraulic effects." *J. Wtrwy, Port, Coast, and Oc. Engrg.*, **123**(4), 149-157.

Driscoll, N. W., Weissel, J. K., Goff, J. A. (2000). "Potential for large-scale submarine slope failure and tsunami generation along the U.S. Mid-Atlantic Coast." Geology (in press).

Edgers, L., and Karlsrud, K. (1982). "Soil flows generated by submarine slides: Case studies and consequences." *Nor. Geotech. Inst. Bull.*, *143*, 1-11.

Fine, I. V., Rabinovich, A. B., Kulikov, E. A., Thomson, R. E., and Bornhold, B. D. (1998). "Numerical modelling of landslide-generated tsunamis with application to the Skagway Harbor tsunami of November 3, 1994." *Proc. Tsunami Symp.*, Paris.

Goldfinger, C., Kulm, L. D., McNeill, L. C., Watts, P. (2000). "Super-scale failure of the Southern Oregon Cascadia Margin." *PAGEOPH,* **157,** 1189-1226.

Grilli, S. T., Skourup, J., and Svendsen, I. A. (1989). "An efficient boundary element method for nonlinear water waves." *Engrg. Analysis Boundary Elements,* **6**(2), 97-107.

Grilli, S. T., Subramanya, R., Svendsen, I. A. and Veeramony, J. (1994) Shoaling of Solitary Waves on Plane Beaches. ." *J. Wtrwy, Port, Coast, and Oc. Engrg.,* **120**(6), **609-628.**

Grilli, S. T., and Subramanya, R. (1996). "Numerical modeling of wave breaking induced by fixed or moving boundaries." *Comp. Mech.*, **17, 374-391.**

Grilli, S. T., Svendsen, I. A., and Subramanya, R. (1998). "Breaking criterion and characteristics for solitary waves on slopes -- Closure." *J. Wtrwy, Port, Coast, and Oc. Engrg.,* **124**(6), **333-335.**

Grilli, S. T., and Watts, P. (1999). "Modeling of waves generated by a moving submerged body: Applications to underwater landslides." *Engrg. Analysis Boundary Elements,* **23**(8), **645-656.**

Hampton, M. A., Lee, H. J., and Locat, J. (1996). "Submarine landslides." *Rev. Geophys.,* **34**(1), *33-59.*

Harbitz, C. B. (1992). "Model simulations of tsunamis generated by the Storegga slides." *Marine Geology*, **105, l-21.**

Heinrich, P. (1992). "Nonlinear water waves generated by submarine and aerial landslides." *J. Wtrwy, Port, Coast, and Oc. Engrg.,* **118**(3), **249-266.**

Imamura, F., and Imteaz, M. M. A. (1995). "Long waves in two-layers: Governing equations and numerical model." *Sci. Tsunami Hazards,* **13**, 3-24.

Imamura, F., and Gica, E. C. (1996). "Numerical model for tsunami generation due to subaqueous landslide along a coast." *Sci. Tsunami Hazards,* **14, 13-28.**

Iwasaki, S. (1982). "Experimental study of a tsunami generated by a horizontal motion of a sloping bottom." *Bull. Earth. Res. Inst., 57, 239-262.*

Iwasaki, S. (1987). "On the estimation of a tsunami generated by a submarine landslide." *Proc., Int. Tsunami Symp.,* Vancouver, B.C., 134-138.

Iwasaki, S. (1997). "The wave forms and directivity of a tsunami generated by an earthquake and a landslide." *Sci. Tsunami Hazards,* **15, 23-40.**

Jiang, L., and LeBlond, P. H. (1992). "The coupling of a submarine slide and the surface waves which it generates." *J. Geoph. Res.,* **97**(C8), *12731-12744.*

Jiang, L., and LeBlond, P. H. (1993). "Numerical modeling of an underwater Bingham plastic mudslide and the waves which it generates." *J. Geoph. Res.,* **98**(C6), 10303-10317.

Jiang, L., and LeBlond, P. H. (1994). "Three-dimensional modeling of tsunami generation due to a submarine mudslide." *J. Phys. Ocean., 24, 559-573.*

Kawata, Y. and International Tsunami Survey Team members. (1999). "Tsunami in papua New guinea was intense as first thought." *Eos, Trans. Am. Geophys. Union,* **80**(9), 101.

Liu, P.L.-F., Synolakis, C. E., Yeh, H. H. (1991). "Tsunami in Papua New Guinea was intense as first thought." *J. Fluid Mech., 229, 675-688.*

Synolakis, C. E., Bardet, J.-P., Borrero, J. C., Davies, H., Grilli, S. T., Okal, E. A., Silver, E., Sweet, S., Tappin, D. R., Watts, P. The Slump Origin of the 1998 Papua New Guinea Tsunami. *Proc. Royal Society,* A (submitted).

Pelinovsky, E., and Poplavsky, A. (1996). "Simplified model of tsunami generation by submarine landslide." *Phys. Chem. Earth,* **21**(12), 13- 17.

Prior, D. B., and Coleman, J. M. (1979). "Submarine landslides: Geometry and nomenclature." *Z. Geomorph. N. F.,* **23**(4), *415-426.*

Tappin, D. R. , Matsumoto, T., and shipboard scientists. (1999). "Offshore surveys identify sediment slump as likely cause of devastating Papua New Guinea tsunami 1998 .", *Eos, Trans. Am. Geophys. Union,* **80**(30), *329.*

Tappin, D. R., Watts, P., McMurtry, G. M., Lafoy, Y., Matsumoto, T. (2000). "The Sissano Papua New Guinea tsunami of July 1998 – Offshore evidence on the source mechanism. ", *Marine Geol.* (in press).

Tuck, E. O., and Hwang, L.-S. (1972). "Long Wave Generation on a Sloping Beach." *J. Fluid Mech.*, **51**(3), **449-461.**

Verriere, M., and Lenoir, M. (1992). "Computation of waves generated by submarine landslides." *Intl. J. Num. Methods Fluids,* **14, 403-421.**

Watts, P. (1997). "Water waves generated by underwater landslides," PhD thesis, California Inst. of Technol., Pasadena, CA.

Watts, P. (1998). "Wavemaker curves for tsunamis generated by underwater landslides." *J. Wtrwy, Port, Coast, and Oc. Engrg.,* **124**(3), *127-137.*

Watts, P. (2000). "Tsunami features of solid block underwater landslides." *J. Wtrwy, Port, Coast, and Oc. Engrg.,* **126**(3), *144-152.*

Watts, P., Grilli, S. T., and Synolakis, C. E. (2000). "Tsunami generation by submarine mass failure. I: Wavemaker models." *J. Wtrwy, Port, Coast, and Oc. Engrg.* (submitted).

Wiegel, R. L. (1955). "Laboratory studies of gravity waves generated by the movement of a submarine body." *Trans. Am. Geophys. Union,* **36**(5), *759-774.*

Yeh, H. H., Liu, P.L.-F., Synolakis, *C.* E. (1996). *Long-wave runup models: Friday Harbor, USA,* 12-17 *Sept.* 1995. World Scientific, Singapore.

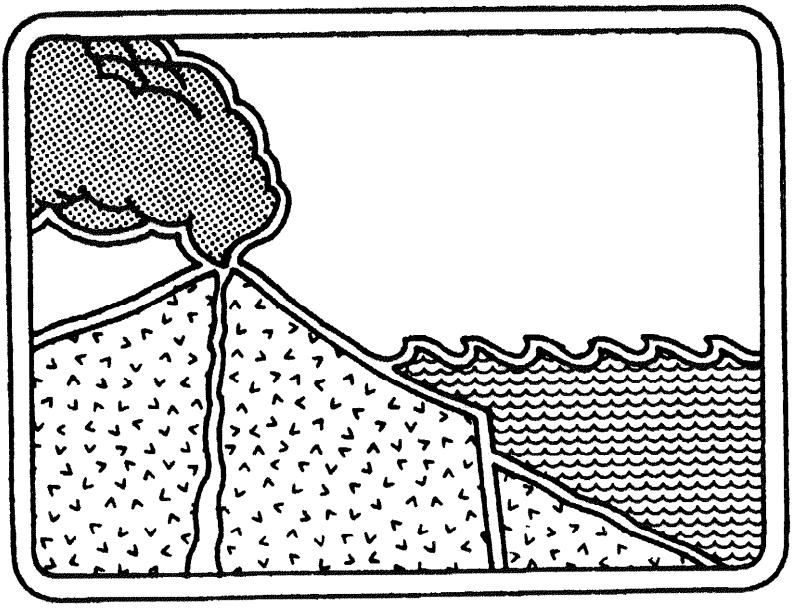

MEMORIUM

SYDNEY 0. WIGEN

Sydney 0. Wigen was a pioneer tsunami researcher in Canada. He died on August *20, 2000* at the age of 77. He lived in Salt Spring Island, BC, Canada.

The two people that got me interested in tsunami research were Gerry Dohler and Syd Wigen. In early 1969 while working with the department of Fisheries and Oceans in Ottawa, my colleague Fred Barber mentioned to me the puzzling result that during the 1964 Alaska earthquake tsunami event, the largest amplitude (outside of Alaska) any where on the Pacific coast of North America, did not occur at the open coastline but well inland at Port Alberni. He asked me to talk to Syd Wigen who was working in Victoria, BC. Syd invited me to visit him which I did in April 1969. I found him to be a very patient and kind person. He drove me to Port Alberni and we spent several hours looking at all the areas inundated by the 1964 tsunami. It was the personal visit to the site that gave me the clue as to why the tsunami amplitude was largest at Port Alberni, which we now attribute to resonance amplification. Since that time I worked closely with Syd on various tsunami problems in Canada, and our colloboration increased after I moved to Victoria in November 1977 and continued till well after his retirement in 1985. He worked very hard in putting together the IUGG tsunami conference, the ITSU meeting and a tsunami workshop in August 1985 in Victoria.

His contributions to the understanding and reduction of tsunami hazards have and will continue to save lives throughout the world.

Tad Murty

TSUNAMI WEB SITE DIRECTORY

A web site with an index of the papers published during the last 18 years of *Science of Tsunami Hazards* is being published by Dr. Antonio Baptista. The web site has the following URL:

http://www.ccalmr.ogi.edu/STH

The journal issues thru Volume 17 in PDF format are available at the following URL:

http://epubs.lanl.gov/tsunami

and on a CD-ROM from the Tsunami Society. A collection of computer generated tsunami animations is also on the CD-ROM.

The International Tsunami Information Center maintains a web site with current information of interest to the Tsunami community. The web site has the following URL:

http://tgsv5.nws.noaa.gov/pr/hq/itic.htm

The West Coast and Alaska Tsunami Warning Center maintains a web site with tsunami information. The web site has the following URL:

http://www.alaska.net/~atwc/

A beautiful web site about Tsunamis is being published by **Tsunami Society** member, Dr. George Pararas-Carayannis. His tsunami web site has the following URL:

http://www.geocities.com/capecanaveral/lab/1029

A web site about The National Tsunami Hazard Mitigation Program is maintained by **PMEL.** The web site has the following URL:

http://www.pmel.noaa.gov/tsunami-hazard

Several members of **The Tsunami Society** have helped develop a web site for the **Pacific Tsunami Museum** in Hilo, Hawaii. The web site has the following URL:

http://planet-hawaii.com/tsunami

A remarkable website by Michael Paine on Tsunamis from Asteroid Impacts from the -Australian perspective has the following URL:

http://www1.tpgi.com.au/users/tps-seti/spacegd7.html

SECOND TSUNAMI SYMPOSIUM

MAY 28, 29, 30, 2002

EAST-WEST CENTER, UH

HONOLULU, HAWAII

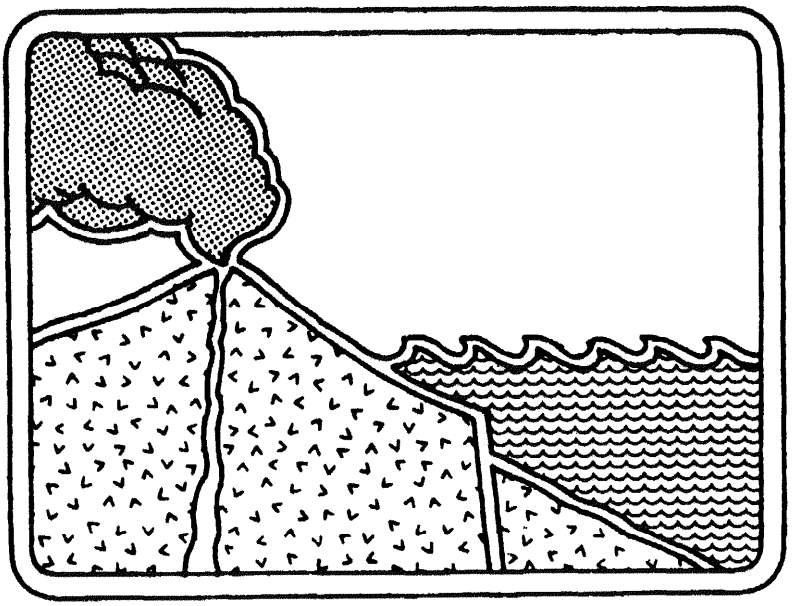

ABSTRACTS DUE - September 1, 2001

PAPERS DUE - January 1, 2002

Send Abstracts and Papers to
Dr. Charles L. Mader
1049 Kamehame Drive
Honolulu, HI 96825 USA
e-mail-MCCOH@juno.com

Application for Membership

THE TSUNAMI SOCIETY
P. 0. Box 37970
Honolulu, Hawaii 96817, USA

I desire admission into the Tsunami Society.

NAME _____

ADDRESS _____

_____

_____

Telephone/FAX _____

E-MAIL ADDRESS _____

Mail Registration to The Tsunami Society, P. 0. Box 37970, Honolulu, Hawaii, 96817, USA. The Membership Fee is $30.00 for individual Members and $100.00 for Institutions. Please make check to"The Tsunami Society".

Send dues for one year with application. Membership shall date from January 1 of the year in which the applicant joins. Membership of an applicant applying on or after October 1 will begin with January 1 or the following calendar year and his first dues payment will be applied to that year.

Membership includes a subscription to the society journal *Science of Tsunami Hazards.*